



MINISTÉRIO DA EDUCAÇÃO

INSTITUTO FEDERAL DO ESPÍRITO SANTO

REITORIA

Avenida Rio Branco, 50 – Santa Lúcia – 29056-264 – Vitória – ES

27 3357-7500

ANEXO VIII

RELATÓRIO DE ATIVIDADES DO AFASTAMENTO PARA PARTICIPAÇÃO EM PROGRAMA DE PÓS-GRADUAÇÃO *STRICTO SENSU*, PÓS-DOUTORADO ESPECIALIZAÇÃO OU ESTÁGIO (PARCIAL OU INTEGRAL)

DADOS DO SERVIDOR

Servidor: Jamile Rocha Pavan	Matrícula Siape: 2453159
Unidade de lotação/exercício: Venda Nova do Imigrante/ Professor EBTT	Setor: Coordenadoria do curso técnico em agroindústria integrado ao ensino médio
E-mail: jamile.pavan@ifes.edu.br	Telefone: 27 995157645

DADOS DA CAPACITAÇÃO

Curso/área: Química	Nível: Doutorado
Instituição: Universidade Federal do Espírito Santo (UFES)	Carga horária/créditos exigidos: 36 créditos (porém foram aproveitados 24 créditos do mestrado)
Semestre referente: 2024/1	Carga horária/créditos realizados: finalizado (total de 40 créditos)

Resumo das atividades realizadas

No semestre 2024/1 foram publicados dois artigos e dedicou-se esse semestre para a finalização da tese.
A defesa ocorreu no dia 06 de agosto de 2024 com aprovação.

Planejamento das atividades do próximo semestre

TRABALHO DE CONCLUSÃO DE CURSO, DISSERTAÇÃO OU TESE (se houver)

Situação	<input type="checkbox"/> Não definida	<input type="checkbox"/> Em projeto	<input type="checkbox"/> Iniciada	<input type="checkbox"/> Em execução	<input checked="" type="checkbox"/> Finalizado
Título Síntese e Caracterização de Complexos de Cobalto com Potencial para Investigação da Tautomeria de Valência					
Data prevista para término: agosto/2024	Orientador Marcos Antônio Ribeiro				

ANEXOS E ASSINATURA

<input type="checkbox"/>	Histórico parcial
<input type="checkbox"/>	Declaração de matrícula
<input checked="" type="checkbox"/>	Outros: declaração de aprovação
DATA	ASSINATURA E CARIMBO/ASSINATURA ELETRÔNICA
DATA	ASSINATURA E CARIMBO DO ORIENTADOR OU COORDENADOR DE CURSO

Síntese e Caracterização de Complexos de Cobalto com Potencial para
Investigação da Tautomeria de Valência.

Jamile Rocha Pavan

Tese submetida ao Programa de Pós-Graduação em Química do Centro de Ciências Exatas da Universidade Federal do Espírito Santo como requisito parcial para a obtenção do Grau de Doutora em Química.

Aprovada em 06/08/2024 por:

Prof. Dr. Marcos Antônio Ribeiro
Orientador
UFES

Profa. Dra. Tatiana Renata Gomes Simões
UFPR

Prof. Dr. Rafael Alves Allão Cassaro
UFRJ

Dr. Maurício Portioli Franco
Unicamp

Prof. Dr. Cleocir José Dalmaschio
UFES

Universidade Federal do Espírito Santo
Vitória, agosto de 2024





UFES
Universidade Federal do Espírito Santo
Centro de Ciências Exatas
Programa de Pós-Graduação em Química
Credenciamento/MEC 0656 de 27/07/2017

85ª ATA DE DEFESA DE TESE DE DOUTORADO EM QUÍMICA

Ata da sessão de defesa da 85ª Tese de Doutorado em Química do Centro de Ciências Exatas da Universidade Federal do Espírito Santo, da aluna Jamile Rocha Pavan, candidata ao grau de Doutora em Química. Às 09:00 horas do dia 06/08/2024, no Miniáudatório do bloco B sala A12, o Presidente da Comissão Examinadora, Prof. Dr. Marcos Antônio Ribeiro – UFES, iniciou a sessão apresentando a Comissão constituída, além dele próprio que é o Orientador, e pelos outros membros que são a Profa. Dra. Tatiana Renata Gomes Simões (Examinadora Externa– UFPR, o Prof. Dr. Rafael Alves Allão Cassaro (Examinador Externo) – UFRJ, o Dr. Maurício Portioli Franco (Examinador Externo) – Unicamp e o Prof. Dr. Cleocir José Dalmaschio (Examinador Interno) – UFES. A seguir, o presidente passou a palavra à candidata que, em 50 minutos, apresentou a sua tese intitulada “Síntese e Caracterização de Complexos de Cobalto com Potencial para Investigação da Tautomeria de Valência.”. Finda a apresentação, o presidente passou a palavra aos membros da Comissão para procederem à arguição do candidato. Finda a arguição, o presidente convidou a Comissão para dirigir-se a uma sala reservada, para deliberação. Após a deliberação, a Comissão retornou e o presidente informou aos presentes que a tese fora aprovada. Logo após, o presidente declarou encerrada a sessão, e eu, Marcos Antônio Ribeiro, lavrei a presente Ata, que é assinada pelos membros da Comissão Examinadora. Vitória, 06/08/2024.

Prof. Dr. Marcos Antônio Ribeiro¹
UFES – Orientador

Profa. Dra. Tatiana Renata Gomes Simões
UFPR – Titular Externo

Prof. Dr. Rafael Alves Allão Cassaro
UFRJ – Titular Externo

Dr. Maurício Portioli Franco
Unicamp– Titular Externo

Prof. Dr. Cleocir José Dalmaschio
UFES – Titular Interno

¹ O documento será assinado eletronicamente em conformidade com as normas prescritas na Portaria Normativa PRPPG/ UFES nº 08/2021.





UNIVERSIDADE FEDERAL DO ESPÍRITO SANTO
Centro de Ciências Exatas
Programa de Pós-Graduação em Química

REGISTRO DE JULGAMENTO DA TESE DO(A) CANDIDATO(A) AO GRAU DE DOUTOR(A) PELO PPGQI/ UFES

A Comissão Examinadora da Tese de Doutorado intitulada “Síntese e Caracterização de Complexos de Cobalto com Potencial para Investigação da Tautomeria de Valência.”, elaborada por Jamile Rocha Pavan, candidato(a) ao Grau de Doutor(a) em Química, recomendou, após a apresentação da Tese realizada no dia 06/08/2024, que ela seja:

Aprovada

Após a deliberação da banca a tese foi aprovada e a candidata procederá com as correções indicadas pela banca. O texto final corrigido será enviado para a banca após análise do orientador.

Reprovada

Os membros da Comissão deverão indicar a natureza de sua decisão através de sua assinatura¹ na coluna apropriada que segue:

Aprovada

Reprovada

Prof. Dr. Marcos Antônio Ribeiro

Profa. Dra. Tatiana Renata Gomes Simões

Prof. Dr. Rafael Alves Allão Cassaro

Dr. Maurício Portioli Franco

Prof. Dr. Cleocir José Dalmaschio

¹ O documento será assinado eletronicamente em conformidade com as normas prescritas na Portaria Normativa PRPPG/ UFES nº 08/2021.





Documentos Defesa Jamile Pavan

Data e Hora de Criação: 08/08/2024 às 13:20:42

Documentos que originaram esse envelope:

- folha_Rosto_defesa_jamile.pdf (Arquivo PDF) - 1 página(s)
- ata_defesa_tese_jamile.pdf (Arquivo PDF) - 1 página(s)
- DocumentosDefesa_Jamile Rocha Pavan.pdf (Arquivo PDF) - 1 página(s)



Hashs únicas referente à esse envelope de documentos

[SHA256]: eb7a181dfda21b0b35dd1cff9d2ceb51c1875cc22852165a1cd733486c71b4fc

[SHA512]: 83b25976bb20f977defd5d484ec71daa30fefff6c02ade0281aec39ffeca04c1080655a5c551b09c88df34a5f87f0b8aa62a8a7e45dbac4108021d545e286cab

Lista de assinaturas solicitadas e associadas à esse envelope



ASSINADO - Rafael Alves Allão Cassaro (allao.cassaro@iq.ufrj.br)

Data/Hora: 09/08/2024 - 03:02:16, IP: 201.17.95.213

[SHA256]: 4898dafbee31d12a0c8e8202701d4b9f0017de4e06d7e0e1be3c46e47db63e2



ASSINADO - Cleocir Jose Dalmaschio (cleocir.dalmaschio@ufes.br)

Data/Hora: 08/08/2024 - 17:29:47, IP: 200.137.65.103

[SHA256]: a365814d9931c9bf846fb5faa38b1816ec69d4fc1f0525b93a434afb9c0ea058



ASSINADO - Marcos Antonio Ribeiro (marcos.a.ribeiro@ufes.br)

Data/Hora: 08/08/2024 - 13:21:15, IP: 200.137.65.107, Geolocalização: [-20.275335, -40.303008]

[SHA256]: 5f7b4fa1103ea0f09c7c44740822d13a9dc3bd50351023813a2170501a833145

Marcos A. Ribeiro



ASSINADO - Maurício Portioli (mpfranco@unicamp.br)

Data/Hora: 08/08/2024 - 13:40:01, IP: 191.254.183.175, Geolocalização: [-22.858956, -47.048294]

[SHA256]: 7cc61f8b924970e3bee110c6a3c415d7b99a8d2eff1f88d6b8032762ae88cf8f



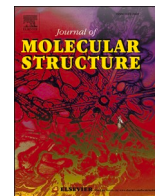
ASSINADO - Tatiana Renata (tatianarenat@gmail.com)

Data/Hora: 12/08/2024 - 17:30:58, IP: 200.17.203.180, Geolocalização: [-25.441075, -49.240473]

[SHA256]: 1874ef42f9f70f121ca5749084a98666e38894faee7e020264f61acba86258e1

Histórico de eventos registrados neste envelope

- 12/08/2024 17:30:58 - Envelope finalizado por tatianarenat@gmail.com, IP 200.17.203.180
- 12/08/2024 17:30:58 - Assinatura realizada por tatianarenat@gmail.com, IP 200.17.203.180
- 12/08/2024 17:30:44 - Envelope visualizado por tatianarenat@gmail.com, IP 200.17.203.180
- 09/08/2024 03:02:16 - Assinatura realizada por allao.cassaro@iq.ufrj.br, IP 201.17.95.213
- 08/08/2024 17:29:47 - Assinatura realizada por cleocir.dalmaschio@ufes.br, IP 200.137.65.103
- 08/08/2024 17:29:26 - Envelope visualizado por cleocir.dalmaschio@ufes.br, IP 200.137.65.103
- 08/08/2024 13:40:01 - Assinatura realizada por mpfranco@unicamp.br, IP 191.254.183.175
- 08/08/2024 13:39:34 - Envelope visualizado por mpfranco@unicamp.br, IP 191.254.183.175
- 08/08/2024 13:21:15 - Assinatura realizada por marcos.a.ribeiro@ufes.br, IP 200.137.65.107
- 08/08/2024 13:20:58 - Envelope registrado na Blockchain por marcos.a.ribeiro@ufes.br, IP 200.137.65.107
- 08/08/2024 13:20:57 - Envelope encaminhado para assinaturas por marcos.a.ribeiro@ufes.br, IP 200.137.65.107
- 08/08/2024 13:20:43 - Envelope criado por marcos.a.ribeiro@ufes.br, IP 200.137.65.107



Unveiling the electronic and molecular structure of a trinuclear ruthenium cluster containing one nitrosyl ligand

Ana Paula de Lima Batista^{a,b,*}, Jamile Rocha Pavan^c, Marcos Antônio Ribeiro^c, Sofia Nikolaou^b

^a Departamento de Química, Grupo Computacional de Catálise e Espectroscopia (GCCE), Universidade Federal de São Carlos (UFSCar), 13565-905, São Carlos, SP, Brazil

^b Departamento de Química, Laboratório de Atividade Biológica e Química Supramolecular de Compostos de Coordenação (LABiQSC2), Faculdade de Filosofia, Ciências e Letras de Ribeirão Preto, Universidade de São Paulo, Av. Bandeirantes 3900, 14040-901, Ribeirão Preto, SP, Brazil

^c Centro de Ciências Exatas, Departamento de Química, Universidade Federal do Espírito Santo (UFES), Avenida Fernando Ferrari, 514, Goiabeiras, 29075-910, Vitória, ES, Brazil

ARTICLE INFO

Keywords:

Multiconfigurational methods
Ru-NO bond
Ruthenium polynuclear systems
DFT
X-ray data

ABSTRACT

The understanding of the Ru-NO bond in Ru nitrosyl systems is of great interest due to the non-innocent nature of the NO ligand, and because of the ability of such compounds to release nitric oxide, an essential physiological regulator. The Ru-NO bond description can be even more complicated when it comes to polynuclear systems such as the μ -oxo clusters of general formula $[\text{Ru}_3\text{O}(\text{CH}_3\text{COO})_6(\text{L})_3]^n$, which can be electronically localized or delocalized themselves depending on the nature of the L ligands, or present unpaired electrons depending on the Ru ions oxidation state. Herein, we present a detailed electronic- and molecular-structure description of the $[\text{Ru}_3\text{O}(\text{CH}_3\text{COO})_6(\text{py})_2\text{NO}]\text{PF}_6$ (py = pyridine) cluster using multiconfigurational approaches and X-ray diffraction analysis. The X-ray data unveil a linear Ru-NO moiety with a Ru-NO angle of 180° . Although most linear $\{\text{RuNO}\}_6$ complexes have been largely described as $\text{Ru}^{\text{II}}\text{-NO}^+$, our valence bond-type analysis based on a CASSCF ground state wavefunction, with an active space comprised of 18 electrons and 16 orbitals, showed a predominance of the $\text{Ru}^{\text{III}}\text{-NO}^\circ$ configuration, with minor contributions from $\text{Ru}^{\text{IV}}\text{-NO}^-$ and $\text{Ru}^{\text{II}}\text{-NO}^+$. These findings provide a more precise framework to rationalize the electronic properties of trinuclear ruthenium nitrosyls, aiding the planning of new NO releasers based on those clusters.

1. Introduction

The exciting electronic and magnetic properties of oxo-carboxylate-bridged polynuclear metal compounds, such as valence-state delocalization, multi-electron redox behavior and magnetic couplings, often enable these systems to mediate various chemical and biological transformations, such as catalyzed reactions, drug delivery, and electron-transfer processes, among others [1–9]. Nowadays, there are a plethora of μ_3 -oxo bridged acetates of general formula $[\text{M}_3\text{O}(\text{CH}_3\text{COO})_6\text{L}_3]^n$ ($\text{M} = d$ block transition metal ion; Ac = acetate; L = range of ligands) and, among them, those based on ruthenium ion have shown great versatility [10,11]. For instance, depending on the choice of the ancillary ligands, the $[\text{Ru}_3\text{O}(\text{CH}_3\text{COO})_6(\text{L})_3]^n$ systems might play a role as anticancer or trypanocidal agents, can show an extended absorption profile, covering the ultraviolet and visible regions, and a rich multi-electron redox behavior for applications in sensors and

electrochromic devices [10,11].

The $[\text{Ru}_3\text{O}(\text{CH}_3\text{COO})_6(\text{L})_2(\text{NO})]^+$ clusters ($\text{L} =$ pyridinic ligands), in particular, are found to be NO delivery systems [12–14], and they have been a subject of interest due to its potential as anticancer and vaso-relaxant agents [14–17]. Nitric oxide (NO) molecule is recognized in various functions within mammalian biology. For instance, NO can act as a neurotransmission and potent vasodilator and promote the death of cancer cells [18–21]. Therefore, many studies have emerged aiming to develop new NO-releasing molecules [15–18,20,22–25].

Toward the design of new trinuclear ruthenium nitrosyl compounds, the $[\text{Ru}_3\text{O}(\text{CH}_3\text{COO})_6(\text{py})_2(\text{NO})]^+$ has been explored [12,14] and, hence, an understanding of its electronic and molecular structures becomes essential. For example, the formal description of this stable nitrosyl cluster as $\text{Ru}^{\text{III}}\text{Ru}^{\text{III}}\text{Ru}^{\text{III}}\text{-NO}^0$ or $\text{Ru}^{\text{III}}\text{Ru}^{\text{III}}\text{Ru}^{\text{II}}\text{-NO}^+$ needs to be clarified. NO is a typical example of a non-innocent ligand that can interact with a metal center as NO^+ , NO^0 , or NO^- , therefore causing

* Corresponding author.

E-mail address: aplbatisa@ufscar.br (A.P. de Lima Batista).

<https://doi.org/10.1016/j.molstruc.2024.138119>

Received 27 September 2023; Received in revised form 16 February 2024; Accepted 20 March 2024

Available online 21 March 2024

0022-2860/© 2024 Elsevier B.V. All rights reserved.

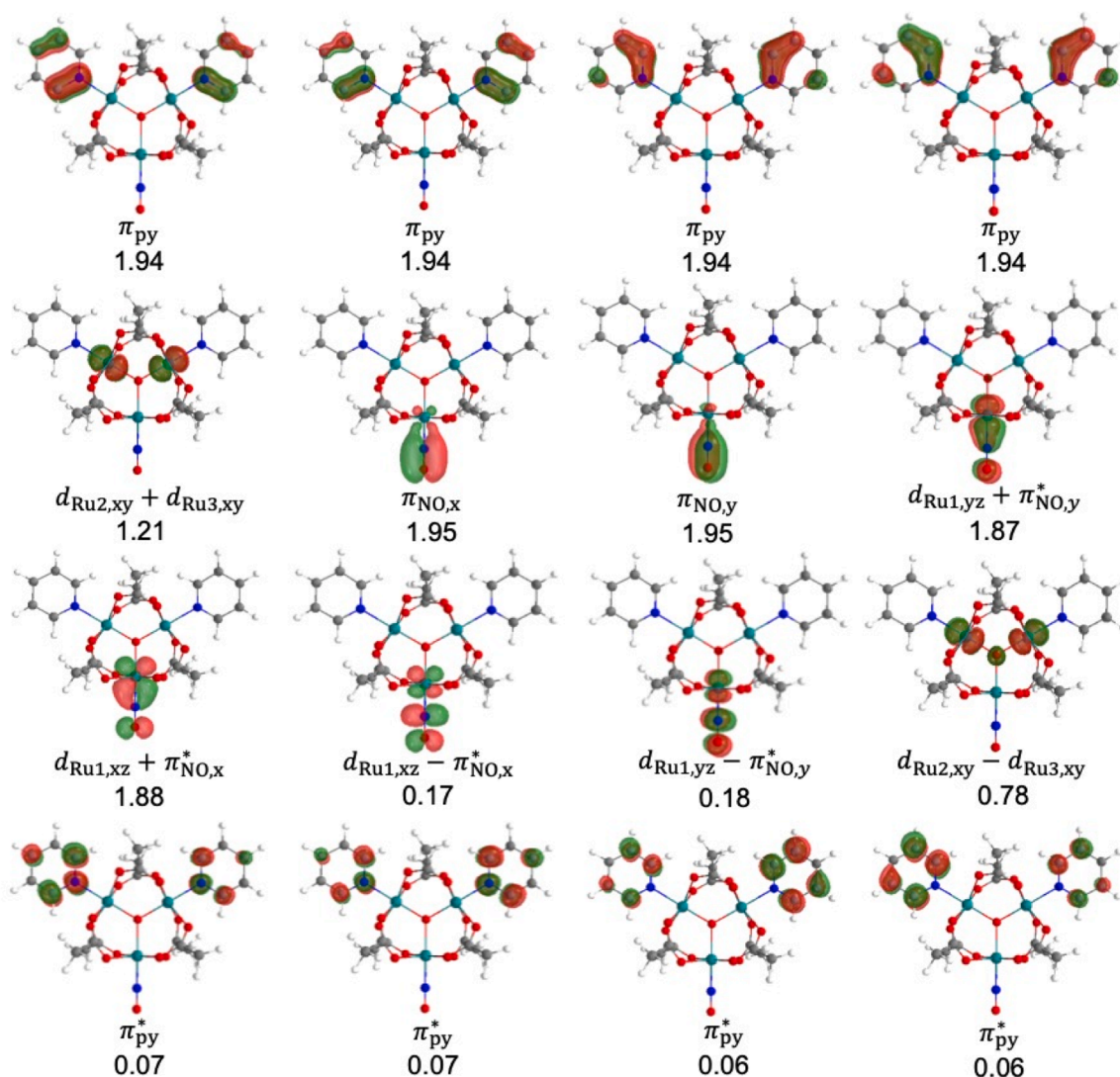


Fig. 1. Active space orbitals and natural occupation numbers (NOONs) in the CAS(18e,16o) calculation of the $[\text{Ru}_3\text{O}(\text{CH}_3\text{COO})_6(\text{py})_2\text{NO}]^+$ cluster in its ground electronic state.

difficulties in resolving the complex electronic structure of nitrosyl systems [13,26–30]. Therefore, the Enemark–Feltham $\{\text{Ru} - \text{NO}\}^n$ notation [31,32], with n being the total number of electrons in the metal d and nitrosyl π^* orbitals, is frequently invoked. However, adopting this framework, it is impossible to assign a particular oxidation state to ruthenium or a formal charge to NO, which is of great interest for understanding the reactivity of such systems. In the case of $[\text{Ru}_3\text{O}(\text{CH}_3\text{COO})_6(\text{py})_2(\text{NO})]\text{PF}_6$, as no EPR signal was seen at either room or liquid nitrogen temperatures, a strong coupling between the available π^* -electron in NO^0 and the ruthenium $d\pi$ -electrons in the $\text{Ru}^{\text{III}}\text{Ru}^{\text{III}}\text{Ru}^{\text{III}}$ cluster was suggested [12].

Furthermore, the occurrence of a given metal-NO bond as linear or bent is frequently associated with NO^+ or NO^0 forms of nitrosyl complexes, respectively [19,33,34]. Initially, it was broadly accepted that most linear $\{\text{Ru}-\text{NO}\}$ moieties were best described as $\text{Ru}^{\text{II}}-\text{NO}^+$. This geometry provides a better overlap between the metal $d\pi$ and NO^+ π^* orbitals, and the lower oxidation state of the metal center, along with the empty π^* orbital on the NO ligand, enable strong π -backbonding interactions. Nevertheless, this relation was later proved to be followed only sometimes [19,29,33,35]. As reported in a recent paper [9], polynuclear complexes containing the $\{\text{Ru}-\text{NO}\}$ unit are still unusual. Due to difficulties in obtaining crystals for the $[\text{Ru}_3\text{O}(\text{CH}_3\text{COO})_6(\text{py})_2(\text{NO})]^+$ system, the Ru-NO configuration has not been undoubtedly clarified

until now.

Quantum chemical methods are valuable tools that can assist in unveiling the electronic and molecular structures of transition metal systems [36–38]. For large molecular systems, such as our target cluster, most studies are based on density functional theory (DFT) [39–41], although it is also possible to find some earlier computational studies on oxo-centered triruthenium complexes employing semiempirical methods [12,14]. Transition metal (TM) complexes, however, are prone to be strongly correlated systems, that is, systems with degenerate or nearly degenerate states, whose electronic structure is better described by more than one electronic configuration [36,42–44]. These systems require another class of computational approaches referred to as multiconfigurational methods. Nowadays, a variety of different approaches are available [44–60], and the choice for one of them depends on the chemical problem to be elucidated. For instance, the multiconfigurational self-consistent field (MCSCF) theory, in particular, the complete active space self-consistent field (CASSCF) method [61], is a well-established method used to investigate transition metal chemistry [26,62–67]. Another efficient approach developed to treat static electron correlation is the density matrix renormalization group (DMRG) [68,69], which enables the calculation of larger active orbitals spaces compared to CASSCF. The DMRG procedure is also a suitable method for treating TM systems [48,49,70–73]. Recently, the MCSCF approach has

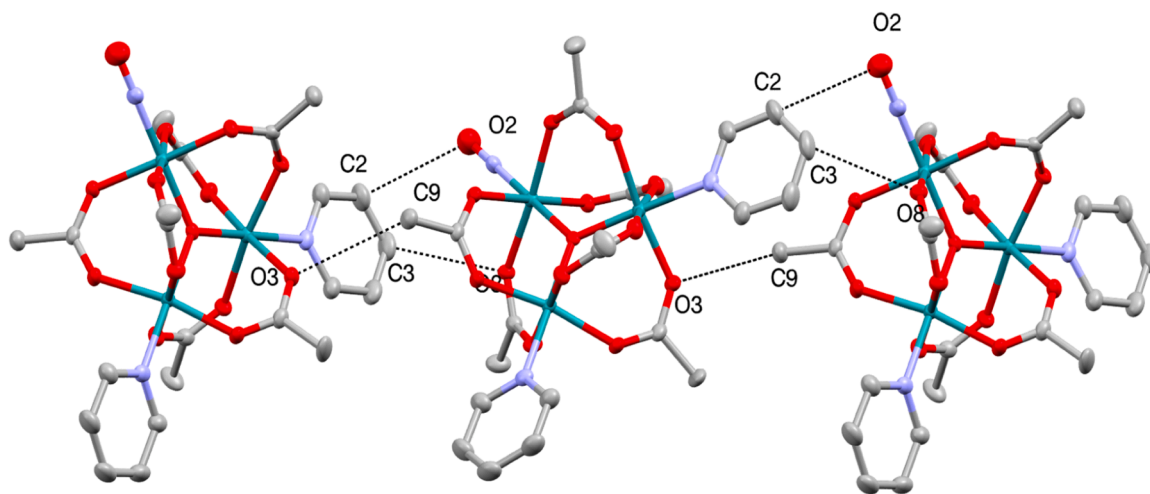


Fig. 3. View of the intermolecular interaction in $[\text{Ru}_3\text{O}(\text{CH}_3\text{COO})_6(\text{NO})(\text{pyridine})_2]^+$. Ellipsoids are drawn with 50 % of probability level and hydrogen atoms are omitted for sake of clarity. Color code: ruthenium is light green, carbon is gray, nitrogen is blue, and oxygen is red.

2.054(2) Å in following the literature [110].

Regarding the NO ligand, the N–O bond distance is 1.144(6) Å. It can be considered equivalent to free NO^0 (1.154 Å) [35], and is much larger than its counterpart NO^+ (1.063 Å) [111], suggesting the presence of NO^0 in the complex. NO^+ has a stronger-acceptor character, in contrast to NO^0 , in which the back donation effect is attenuated by the presence of the π^* unpaired electron. However, in our trinuclear system, the NO^0 π^* electron can stabilize the whole species by coupling with the unpaired electron of the $[\text{Ru}_3\text{O}]^+$, as we discuss in the next section. The Ru–N_{NO} bond distance is 1.752(4) Å, a value shorter than the Ru–N_{pyridine} bond distance, 2.077(3) Å, hence pointing to a stronger bond between Ru and NO ligand. The cluster structure also features a Ru–NO angle of 180° in other words: compared to previously reported Ru–NO systems [26,111–113], the bond distance is consistent with NO^0 , while the bond angle is more typical of NO^+ .

An exciting feature of the X-ray data is the occurrence of non-conventional hydrogen bonds. This kind of interaction has been observed previously for trinuclear carbonyl clusters [114] and, in the case of the nitrosyl investigated here, it is responsible for the occurrence of an organized linear structure, Fig. 3. Each $[\text{Ru}_3\text{O}(\text{CH}_3\text{COO})_6(\text{py})_2\text{NO}]^+$ moiety interacts with the nearest neighbor molecule through a non-conventional hydrogen bond [115,116], where the oxygen from one acetate bridge acts as an acceptor interacting with a hydrogen atom from a methyl group from a neighbor molecule. Besides, the hydrogen atom from the pyridyl ligand also interacts with oxygen from acetate and with oxygen from the nitrosyl ligand. The PF_6^- counter-anion interacts with only hydrogen atoms from acetate. It is arranged in a cage-like structure, where the acetates are spherically distributed, indicating that the anion operates only as a charge-neutralizing agent. The hydrogen bond parameters are shown in Table S3.

A comparison between the DFT-optimized and the X-ray $[\text{Ru}_3\text{O}(\text{CH}_3\text{COO})_6(\text{py})_2\text{NO}]^+$ structures allows one to check the adequacy of the level of theory used to obtain the geometry of the current trinuclear cluster. Three types of errors were adopted to perform this comparison: the RMSE (root mean square error), MUE (mean unsigned error), and MSE (mean signed error) analyses between the DFT and the X-ray structure. The RMSE is obtained from the difference between the two sets of Cartesian coordinates, while the MUE and MSE come from comparing interatomic distances between the two structures. See the supplementary material for more details on these analyses. The RMSE, MUE, and MSE values are, respectively, 0.269, 0.121, and 0.054 Å, showing that our level of theory is appropriate to obtain the molecular structure of $[\text{Ru}_3\text{O}(\text{CH}_3\text{COO})_6(\text{py})_2\text{NO}]^+$. Typical RMSE values reported

for comparisons between experimental and theoretical involving all the Cartesian coordinates of transition metal complexes are within the 0.20–0.35 Å range [84]. At this point, it is also worth mentioning that the geometry of a transition metal center is influenced by its surroundings. Hence, the structures in a crystal differ from that in a discrete molecule. The MUE and MSE errors obtained in terms of interatomic distances allow us to evaluate, in a systematic way, bond length over/under-estimation in our analysis. These last two errors indicate an overestimation of our theoretical interatomic distances.

In addition, because it is not trivial to determine the position of light elements in the presence of heavier ones [84,117,118] we carried out a second analysis, in which the H atoms were excluded. In this latter case, the obtained errors are 0.078, 0.039, and 0.020 Å for the RMSE, MUE, and MSE, respectively. Therefore, the primary source of error in our calculation comes from the position of the H atoms. As the description of the Ru_3O –NO part is of great importance for structural and electronic reasons, an analysis focused only on this part of our system was performed. They corroborated the quality of our optimized geometry. As expected, the errors are the lowest, 0.022, 0.025, and 0.009 Å, respectively, for the RMSE, MUE, and MSE. For instance, the DFT Ru–N_{NO} bond distance is 1.757 Å, only 0.005 Å larger than the X-ray one, while the computed N–O bond length is 0.017 Å shorter than the corresponding experimental value. Based on the error analysis, one can verify that the current optimized structure is adequate. Hence, it was adopted to perform the multiconfigurational single-point calculations in the next step of the current study.

3.2. The electronic structure of $[\text{Ru}_3\text{O}(\text{CH}_3\text{COO})_6(\text{py})_2\text{NO}]^+$

To gain an understanding of the Ru–NO interaction of the $[\text{Ru}_3\text{O}(\text{CH}_3\text{COO})_6(\text{py})_2\text{NO}]^+$, we start focusing on the natural orbitals and the principal configurations of our CAS(18e,16o) wavefunction of the singlet ground electronic state, S_0 . As revealed by the MCPDFT calculations, the triplet electronic state (using the same active space) is 4.5 kcal mol⁻¹ higher in energy, which is consistent with the silent EPR profile observed for $[\text{Ru}_3\text{O}(\text{CH}_3\text{COO})_6(\text{py})_2\text{NO}]^+$ at 77 K [12].

The current active space includes all orbitals with single-orbital entropy larger than 0.20, i.e., orbitals relevant to describing the multiconfigurational character of our system. The CASSCF data in Fig. 1 shows that only the Ru1 atom directly interacts with the NO ligand. The $4d_{xz}$ and $4d_{yz}$ orbitals of Ru1 interact with the π^* orbitals of NO, generating four new orbitals, the $d_{\text{Ru}1,\text{yz}} + \pi_{\text{NO},\text{y}}^*$ and $d_{\text{Ru}1,\text{xz}} + \pi_{\text{NO},\text{x}}^*$ bonding orbitals, and the $d_{\text{Ru}1,\text{xz}} - \pi_{\text{NO},\text{x}}^*$ and $d_{\text{Ru}1,\text{yz}} - \pi_{\text{NO},\text{y}}^*$ antibonding ones. These orbitals are delocalized, suggesting a covalent interaction

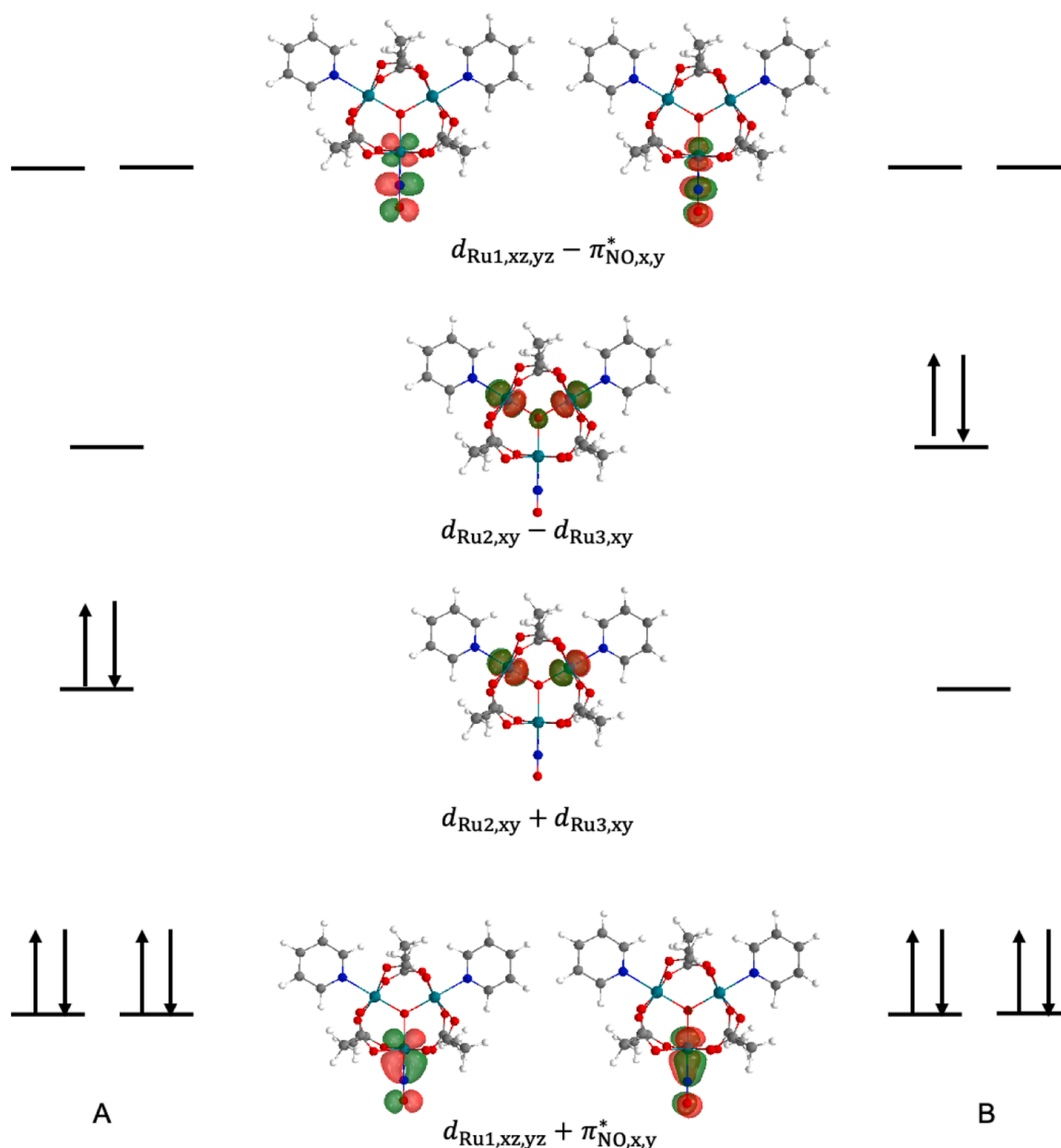


Fig. 4. The two most important configurations expressed in terms of CASSCF natural orbitals for the ground electronic state of the $[\text{Ru}_3\text{O}(\text{CH}_3\text{COO})_6(\text{py})_2\text{NO}]^+$ cluster: Configurations with 45 % (A) and 29 % (B) of the ground electronic state wavefunction. The other natural orbitals are not shown because they remain doubly occupied or unoccupied in these configurations.

between $\text{NO } \pi^*$ and Ru 4d. Furthermore, their associated NOONs deviate from 2 or 0, indicating the presence of static correlation in the Ru-NO bond, reinforcing the need for a multiconfigurational treatment of this interaction. The Ru($4d_{xz}$)-NO(π^*) interaction also presents a minor diradical character, 15.5 %, as calculated using the NOONs of the two orbitals (bonding and antibonding) involved in the bond [66,119–122].

Based on the CASSCF wavefunction expressed in terms of the natural orbitals, the occupation numbers in the ground electronic state most closely resemble the following occupation pattern:

$$\dots (d_{\text{Ru}2,\text{xy}} + d_{\text{Ru}3,\text{xy}})^2 (d_{\text{Ru}1,\text{yz}} + \pi_{\text{NO},\text{y}}^*)^2 (d_{\text{Ru}1,\text{xz}} + \pi_{\text{NO},\text{x}}^*)^2 (d_{\text{Ru}2,\text{xy}} - d_{\text{Ru}3,\text{xy}})^0$$

This major configuration, schematically presented in Fig. 4A, accounts for approximately 45 % of the ground electronic state wavefunction, a weight much lower than expected for a single configurational system (over 90 %). The second most crucial configuration, 29 % of the CASSCF wavefunction (Fig. 4B), can be written as

$$\dots (d_{\text{Ru}2,\text{xy}} + d_{\text{Ru}3,\text{xy}})^0 (d_{\text{Ru}1,\text{yz}} + \pi_{\text{NO},\text{y}}^*)^2 (d_{\text{Ru}1,\text{xz}} + \pi_{\text{NO},\text{x}}^*)^2 (d_{\text{Ru}2,\text{xy}} - d_{\text{Ru}3,\text{xy}})^2$$

The remaining ≈ 26 % of the wave function involves many other configurations, each with weights below 2 %. Table S1 of the supplementary material presents all the generated configurations with CI coefficients larger than 0.05. These data also point to the need to use multiconfigurational approaches to deal with the ground state electronic structure of the $[\text{Ru}_3\text{O}(\text{CH}_3\text{COO})_6(\text{py})_2\text{NO}]^+$ cluster. One notes that in these two major configurations the $d_{\text{Ru}1,\text{yz}} + \pi_{\text{NO},\text{y}}^*$ and $d_{\text{Ru}1,\text{xz}} + \pi_{\text{NO},\text{x}}^*$ bonding orbitals remain doubly occupied, while the $d_{\text{Ru}2,\text{xy}} + d_{\text{Ru}3,\text{xy}}$ bonding orbital and its corresponding antibonding one, $d_{\text{Ru}2,\text{xy}} - d_{\text{Ru}3,\text{xy}}$, alternate their occupation.

Due to the delocalized nature of the d Ru orbitals that interact with the NO ligand and the need to properly assign the electrons to either Ru or NO, hence discussing the NO character in the Ru_3O cluster, we

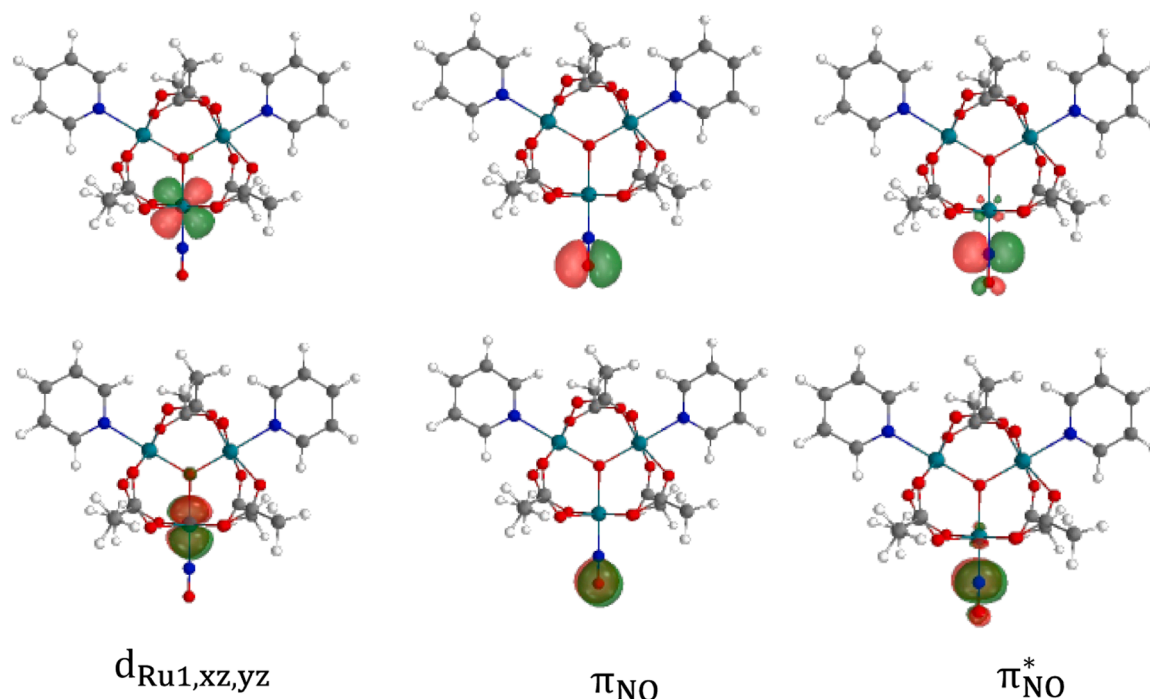


Fig. 5. Localized molecular orbitals involved in the Ru1($4d_{xz,yz}$) and NO (π and π^*) interaction.

Table 2

Analysis of the CASCI wavefunction in terms of the Ru1–NO resonance structures. Contributions of all configurations with coefficients larger than 0.0005 for the ground electronic state (S_0) with different electronic configurations for both Ru1 and NO are considered.

Character	Contribution to S_0 (%)
Ru ^{IV} (d^4)-NO ⁻	8.0
Ru ^{III} (d^5)-NO ⁰	70.4
Ru ^{II} (d^6)-NO ⁺	20.4
Ru ^{II} (d^6)-NO ⁰	0.1

employ the CASCI expansion in terms of localized orbitals. This procedure allows one to perform a valence bond-type analysis of the multiconfigurational ground-state wavefunction of the $[\text{Ru}_3\text{O}(\text{CH}_3\text{COO})_6(\text{py})_2\text{NO}]^+$ cluster, providing more concrete information regarding the NO character in this trinuclear system. In fact, this approach has been previously used to investigate the electronic structure of a series of nitrosyl mononuclear metal complexes [29,66,123]. The localized orbitals of interest for performing the Ru1–NO analysis are depicted in Fig. 5, and they were taken from the Cholesky localization procedure over our active space. The Cholesky algorithm has been adopted due to its success in performing such valence bond-type analysis [119,123,124].

The characterization of electronic structure based on the localized orbitals intends to identify the various resonance structures, such as Ru^{III}(d^5)-NO⁰ or Ru^{II}(d^6)-NO⁺, that account for our ground electronic state. The current transformation of configuration state functions (CSFs) into the basis of localized orbitals resulted in a very diffuse expansion, with many configurations with low weights, all below 5%. Hence, we analyze the results by obtaining the collective weights of all the configurations related to a particular resonance structure, as shown in Table 2. This classification was based on the occupancy of orbitals of predominant Ru1 $4d_{xz,yz}$ and NO (π and π^*) characters. All the CSFs with a coefficient larger than 0.0005 were included in this analysis, which can reproduce approximately 99% of the CASCI wavefunction.

Table 2 shows the Ru^{III}-NO⁰ as the predominant resonance structure

in our ground electronic state system; it has the largest collective weight, about 70%. The second most important contribution comes from the Ru^{II}-NO⁺ character, which accounts for about 20% of our CASCI wavefunction. The Ru^{IV}-NO⁻ resonance structure, on the other hand, contributes only 8%. From these results, we obtain a formal oxidation state of 2.88 for Ru1, i.e., the contributions from the Ru^{IV} are practically canceled out by Ru^{II} one. In an attempt to follow the Enemark–Feltham nomenclature, we can view our polynuclear complex as a $\text{Ru}_2\text{O}\{\text{Ru}(\text{NO})\}_6^+$ system ($\approx 98\%$ of our wavefunction), in which the Ru^{III}-NO⁰ configurations are the most significant. Hence, although most linear $\{\text{RuNO}\}_6^+$ complexes have been largely described as Ru^{II}-NO⁺ [33], we see that our system is closer to a Ru^{III}-NO⁰, which also describes a bond with a major covalent character. Since the Ru^{III}-NO⁰ is the predominant resonance structure, we can recognize why the observed $\nu(\text{NO})$ vibrational frequency (1865 cm^{-1}) is close to that of the NO⁰ as well as the N–O bond distance of $1.148(6)\text{ \AA}$ that we found in our X-ray data. The data presented in Table 2 are consistent with the IR spectroelectrochemical measurements [12,13] that suggested a mixture of Ru^{III}-Ru^{III}-Ru^{III}-NO⁰ and Ru^{III}-Ru^{III}-Ru^{II}-NO⁺ configurations to the $[\text{Ru}_3\text{O}(\text{CH}_3\text{COO})_6(\text{py})_2\text{NO}]^+$ cluster. In fact, a complex $\{\text{Ru}(\text{NO})\}_6^+$ electronic structure, comprised of different resonance structures, has also been described for ruthenium mononuclear systems [29,35,67]. Now, by employing a multiconfigurational approach to a gas-phase $[\text{Ru}_3\text{O}(\text{CH}_3\text{COO})_6(\text{py})_2\text{NO}]^+$ structure, we quantify these contributions for the first time.

The computational approaches used here are multiconfigurational methods that allow one to go beyond the semiempirical calculations that have been applied until now for understanding the $[\text{Ru}_3\text{O}(\text{CH}_3\text{COO})_6(\text{py})_2\text{NO}]^+$ electronic structure or the single-configurational framework of DFT that has been utilized to investigate others trinuclear ruthenium clusters [39,40,125–127]. This type of study has important implications for transition-metal and bioinorganic chemistry because the understanding of the electronic and molecular structure of this cluster is a fundamental step towards the rationalization of its reactivity, the bond between atoms, its role as a new metallodrug and the potential of trinuclear ruthenium family as building blocks of different supramolecular systems [8,10,13,40,41,127–133].

4. Conclusion

The use of X-ray diffraction analysis and multiconfigurational approaches revealed, for the first time, the molecular and electronic structure of the $[\text{Ru}_3\text{O}(\text{CH}_3\text{COO})_6(\text{py})_2\text{NO}]^+$ cluster. According to the crystallographic data, this polynuclear system is characterized by a linear Ru–NO bond with a distance closer to the ones observed for NO^0 .

According to the localized CAS(18e,16o) calculation, the formal oxidation state of the ruthenium in Ru–NO bond is 2.88, and our polynuclear complex can be seen as a $\text{Ru}_2\text{O}\{\text{Ru}(\text{NO})\}^6$ system in which the $\text{Ru}^{\text{III}}\text{--NO}^0$ configurations are the most significant, about 70 %. Hence, although most linear $\{\text{RuNO}\}^6$ complexes have been largely described as $\text{Ru}^{\text{II}}\text{--NO}^+$, the $[\text{Ru}_3\text{O}(\text{CH}_3\text{COO})_6(\text{py})_2\text{NO}]^+$ system is closer to a $\text{Ru}^{\text{III}}\text{--NO}^0$, which also describes a bond with a significant covalent character. Since the ground electronic state is strongly correlated, a multiconfigurational approach is required to describe it adequately.

The $\text{Ru}^{\text{III}}\text{NO}^0$, quantified for the first time in this work, has a predominant resonance structure that is consistent with the experimentally observed $\nu(\text{NO})$ vibrational frequency (1865 cm^{-1}) and the N–O bond distance of $1.144(6)\text{ \AA}$ that we found in our X-ray data. Furthermore, the multiconfigurational data reported in this work is also consistent with the IR spectroelectrochemical measurements that suggested a mixture of $\text{Ru}^{\text{III}}\text{Ru}^{\text{III}}\text{Ru}^{\text{III}}\text{--NO}^0$ and $\text{Ru}^{\text{III}}\text{Ru}^{\text{III}}\text{Ru}^{\text{II}}\text{--NO}^+$ configurations to the $[\text{Ru}_3\text{O}(\text{CH}_3\text{COO})_6(\text{py})_2\text{NO}]^+$ cluster.

CRediT authorship contribution statement

Ana Paula de Lima Batista: Conceptualization, Data curation, Formal analysis, Funding acquisition, Investigation, Methodology, Resources, Software, Validation, Visualization, Writing – original draft, Writing – review & editing. **Jamile Rocha Pavan:** Formal analysis, Visualization, Writing – review & editing. **Marcos Antônio Ribeiro:** Formal analysis, Methodology, Software, Writing – original draft, Writing – review & editing. **Sofia Nikolaou:** Conceptualization, Formal analysis, Supervision, Writing – original draft, Writing – review & editing.

Declaration of competing interest

The authors declare that they have no known competing financial interests or personal relationships that could have appeared to influence the work reported in this paper.

Data availability

Data will be made available on request.

Data availability

The data that support the discussion along with this manuscript findings are available within the main text and its supplementary material.

Acknowledgments

A.P.d.L.B and S.N. acknowledge the São Paulo Research Foundation (FAPESP) (Grants 2018/18060–3, 2022/03478–8, 2022/12043–5, 2021/00675–4), the support of the High-Performance Computing of Universidade de São Paulo (HPC-USP). A.P.d.L.B, J.R.P., M.A.R., and S. N. thanks the Coordenação de Aperfeiçoamento de Pessoal de Nível Superior, finance code 001 (CAPES), and the Conselho Nacional de Desenvolvimento Científico e Tecnológico (CNPq) (Grant 305761/2021–8). M. A. R. and J. R. P. thanks to Fundação de Amparo à Pesquisa e Inovação do Espírito Santo (Grant 922/2023).

Supplementary materials

Supplementary material associated with this article can be found, in the online version, at [doi:10.1016/j.molstruc.2024.138119](https://doi.org/10.1016/j.molstruc.2024.138119).

References

- [1] A. Dikhtiarenko, S. Khainakov, J.R. García, J. Gimeno, Mixed-valence μ_3 -oxo-centered triruthenium cluster $[\text{Ru}_3(\text{II,III,III})(\mu_3\text{-O})(\mu\text{-CH}_3\text{CO}_2)_6(\text{H}_2\text{O})_3]\cdot 2\text{H}_2\text{O}$: synthesis, structural characterization, valence-state delocalization and catalytic behavior, *Inorg. Chim. Acta* 454 (2017) 107–116. <https://www.sciencedirect.com/science/article/pii/S0020169316302882>.
- [2] S.A. Fouda, G.L. Rempel, μ_3 -Oxo-triruthenium acetate cluster complexes as catalysts for olefin hydrogenation, *Inorg. Chem.* 18 (1979) 1–8. <https://doi.org/10.1021/ic50191a001>.
- [3] C. Bilgrien, S. Davis, R.S. Drago, The selective oxidation of primary alcohols to aldehydes by oxygen employing a trinuclear ruthenium carboxylate catalyst, *J. Am. Chem. Soc.* 109 (1987) 3786–3787.
- [4] J.L. Chen, L.Y. Zhang, Z.N. Chen, L. Bin Gao, M. Abe, Y. Sasaki, Syntheses, structures, and redox properties of dimeric triruthenium clusters bridged by bis (diphenylphosphino)acetylene and -ethylene, *Inorg. Chem.* 43 (2004) 1481–1490. <https://doi.org/10.1021/ic0344968>.
- [5] J.W. de Boer, W.R. Browne, B.L. Feringa, R. Hage, Carboxylate-bridged dinuclear manganese systems – from catalases to oxidation catalysis, *C. R. Chim.* 10 (2007) 341–354. <https://doi.org/10.1016/j.crci.2006.09.018>.
- [6] S.P. Pali, D.E. Richardson, M.L. Hansen, B.B. Iversen, F.K. Larsen, L. Singerean, G.A. Timco, N.V. Gerbeleu, K.R. Jennings, J.R. Eyler, Mixed-terminal-ligand oxo-centered carboxylate-bridged trinuclear complexes: gas phase generation by means of electrospray ionization FT-ICR MS, condensed phase synthesis, and X-ray structure of $\text{K}^+[\text{Cr}_3\text{O}(\text{C}_6\text{H}_5\text{COO})_6(\text{F})_2(\text{H}_2\text{O})] - 2(\text{CH}_3)_2\text{CO}$, *Inorg. Chim. Acta* 319 (2001) 23–42. [https://doi.org/10.1016/S0020-1693\(01\)00444-3](https://doi.org/10.1016/S0020-1693(01)00444-3).
- [7] L. Keeney, M.J. Hynes, Kinetics and mechanisms of the electron transfer reactions of oxo-centred carboxylate bridged complexes, $[\text{Fe}_3(\mu_3\text{-O})(\text{O}_2\text{CR})_6\text{L}_3]\text{ClO}_4$, with verdazyl radicals in acetonitrile solution, *Dalton Trans.* (2005) 1524–1531. <https://doi.org/10.1039/B418809H>.
- [8] I. Stepanenko, M. Zalibera, D. Schaniel, J. Telsler, V.B. Arion, Ruthenium-nitrosyl complexes as NO-releasing molecules, potential anticancer drugs, and photoswitches based on linkage isomerism, *Dalton Trans.* 51 (2022) 5367–5393. <https://doi.org/10.1039/D2DT00290F>.
- [9] I. Stepanenko, P. Mizetskiy, E. Orłowska, L. Bućinský, M. Zalibera, B. Vénosová, M. Clémancey, G. Blondin, P. Rapta, G. Novitich, W. Schrader, D. Schaniel, Y.-S. Chen, M. Lutz, J. Kozíšek, J. Telsler, V.B. Arion, The ruthenium nitrosyl moiety in clusters: trinuclear linear μ -hydroxido magnesium(II)-diruthenium(II), μ_3 -oxido trinuclear diiron(III)-ruthenium(II), and tetranuclear μ_4 -oxido trigallium(III)-ruthenium(II) complexes, *Inorg. Chem.* 61 (2022) 950–967. <https://doi.org/10.1021/acs.inorgchem.1c03011>.
- [10] S. Nikolaou, L.G.A. do Nascimento, A.D.P. Alexiou, Oxo-centered trinuclear ruthenium acetates: structure and applications, *Coord. Chem. Rev.* 494 (2023) 215341. <https://doi.org/10.1016/j.ccr.2023.215341>.
- [11] H.E. Toma, K. Araki, A.D.P. Alexiou, S. Nikolaou, S. Dovidauskas, Monomeric and extended oxo-centered triruthenium clusters, *Coord. Chem. Rev.* 219–221 (2001) 187–234. [https://doi.org/10.1016/S0010-8545\(01\)00326-5](https://doi.org/10.1016/S0010-8545(01)00326-5).
- [12] H.E. Toma, A.D.P. Alexiou, S. Dovidauskas, Extended electronic interactions in a triangular μ -oxotriruthenium acetate cluster containing nitric oxide, *Eur. J. Inorg. Chem.* (2002) 3010–3017. [https://doi.org/10.1002/1099-0682\(200211\)2002:11<3010::AID-EJIC3010>3.0.CO;2-L](https://doi.org/10.1002/1099-0682(200211)2002:11<3010::AID-EJIC3010>3.0.CO;2-L).
- [13] N.A.P. dos Santos, A.B. Silva, C.F.N. da Silva, A.D.P. Alexiou, S. Nikolaou, A novel triruthenium nitrosyl bearing a quinolinic ligand: a comparison of its spectroscopic behavior with its pyridine analogues, *New J. Chem.* 46 (2022) 4819–4826. <https://doi.org/10.1039/D1NJ05849E>.
- [14] H.E. Toma, A.D.P. Alexiou, A.L.B. Formiga, M. Nakamura, S. Dovidauskas, M. N. Eberlin, D.M. Tomazela, A nitric oxide releaser based on the μ -oxo-hexaacetate-bis(4-methylpyridine)triruthenium nitrosyl complex, *Inorg. Chim. Acta* 358 (2005) 2891–2899. <https://doi.org/10.1016/j.ica.2004.08.004>.
- [15] N. Cacita, B. Possato, C.F.N. da Silva, M. Paulo, A.L.B. Formiga, L.M. Bendhack, S. Nikolaou, Investigation of a novel trinuclear μ -oxo ruthenium complex as a potential nitric oxide releaser for biological purposes, *Inorg. Chim. Acta* 429 (2015) 114–121. <https://doi.org/10.1016/J.ICA.2015.01.038>.
- [16] Z.A. Carneiro, J.C. Biazotto, A.D.P. Alexiou, S. Nikolaou, Nitric oxide photorelease from a trinuclear ruthenium nitrosyl complex and its in vitro cytotoxicity against melanoma cells, *J. Inorg. Biochem.* 134 (2014) 36–38. <https://doi.org/10.1016/J.JINORGBIO.2014.01.012>.
- [17] C.F.N. da Silva, B. Possato, L.P. Franco, L.C.B. Ramos, S. Nikolaou, The role of ancillary ligand substituents in the biological activity of triruthenium-NO complexes, *J. Inorg. Biochem.* 186 (2018) 197–205. <https://doi.org/10.1016/j.jinorgbio.2018.05.021>.
- [18] N. Lehnert, E. Kim, H.T. Dong, J.B. Harland, A.P. Hunt, E.C. Manickas, K. M. Oakley, J. Pham, G.C. Reed, V.S. Alfaro, The biologically relevant coordination chemistry of iron and nitric oxide: electronic structure and reactivity, *Chem. Rev.* 121 (2021) 14682–14905. <https://doi.org/10.1021/acs.chemrev.1c00253>.
- [19] J.A. McCleverty, Chemistry of nitric oxide relevant to biology, *Chem. Rev.* 104 (2004) 403–418. <https://doi.org/10.1021/cr020623q>.

- [20] E. Muniz Carvalho, E.H. Silva Sousa, V. Bernardes-Génisson, L. de França Lopes, When NO is not enough: chemical systems, advances and challenges in the development of no. and hno donors for old and current medical issues, *Eur. J. Inorg. Chem.* 2021 (2021) 4316–4348.
- [21] Y. Yang, Z. Huang, L.-L. Li, Advanced nitric oxide donors: chemical structure of NO drugs, NO nanomedicines and biomedical applications, *Nanoscale* 13 (2021) 444–459, <https://doi.org/10.1039/D0NR07484E>.
- [22] J.M. Mir, B.A. Malik, R.C. Maturya, Nitric oxide-releasing molecules at the interface of inorganic chemistry and biology: a concise overview, *Rev. Inorganic Chem.* 39 (2019) 91–112, <https://doi.org/10.1515/revic-2018-0017>.
- [23] E. Tfouni, D.R. Truzzi, A. Tavares, A.J. Gomes, L.E. Figueiredo, D.W. Franco, Biological activity of ruthenium nitrosyl complexes, *Nitric Oxide* 26 (2012) 38–53, <https://doi.org/10.1016/j.niox.2011.11.005>.
- [24] P.C. Ford, Y. Shiro, R. van Eldik, Renaissance in NO chemistry, *Inorg. Chem.* 60 (2021) 15831–15834, <https://doi.org/10.1021/acs.inorgchem.1c03287>.
- [25] P.C. Ford, Photochemical delivery of nitric oxide, *Nitric Oxide* 34 (2013) 56–64, <https://doi.org/10.1016/j.niox.2013.02.001>.
- [26] A.P. de Lima Batista, A.G.S. de Oliveira-Filho, S.E. Galembeck, Photophysical properties and the NO photorelease mechanism of a ruthenium nitrosyl model complex investigated using the CASSCF-in-DFT embedding approach, *Phys. Chem. Chem. Phys.* 19 (2017) 13860–13867, <https://doi.org/10.1039/C7CP01642E>.
- [27] G.F. Caramori, A.G. Kunitz, K.F. Andriani, F.G. Doro, G. Frenking, E. Tfouni, The nature of Ru–NO bonds in ruthenium tetraazamacrocyclic nitrosyl complexes—a computational study, *Dalton Trans.* 41 (2012) 7327, <https://doi.org/10.1039/c2dt12094a>.
- [28] G.L. Silva Rodrigues, W.R. Rocha, Nature of the bond, reduction potential, and solvation properties of ruthenium nitrosyl complexes of the type trans-[Ru(NH₃)₄(L)(NO)]^{2+/3+} and [Ru(salen)(L)(NO)]^{2+/3+} in different charge and spin states, *Int. J. Quantum Chem.* 121 (2021) e26476.
- [29] L. Freitag, S. Knecht, S.F. Keller, M.G. Delcey, F. Aquilante, T. Bondo Pedersen, R. Lindh, M. Reiher, L. González, Orbital entanglement and CASSCF analysis of the Ru–NO bond in a Ruthenium nitrosyl complex, *Phys. Chem. Chem. Phys.* 17 (2015) 14383–14392, <https://doi.org/10.1039/C4CP05278A>.
- [30] J.E.M.N. Klein, B. Miehlich, M.S. Holzwarth, M. Bauer, M. Milek, M. M. Khushiyarov, G. Knizia, H.-J. Werner, B. Plietker, The electronic ground state of [Fe(CO)₃(NO)]⁺: a spectroscopic and theoretical study, *Angew. Chem. Int. Ed.* 53 (2014) 1790–1794.
- [31] J.H. Enemark, R.D. Feltham, Principles of structure, bonding, and reactivity for metal nitrosyl complexes, *Coord. Chem. Rev.* 13 (1974) 339–406, [https://doi.org/10.1016/S0010-8545\(00\)80259-3](https://doi.org/10.1016/S0010-8545(00)80259-3).
- [32] J.H. Enemark, R.D. Feltham, Stereochemical control of valence. II. Behavior of the {MNO}⁺ [metal mononitrosyl] group in ligand fields, *J. Am. Chem. Soc.* 96 (1974) 5002–5004, <https://doi.org/10.1021/ja00822a057>.
- [33] M.J. Rose, P.K. Mascharak, Photoactive ruthenium nitrosyls: effects of light and potential application as NO donors, *Coord. Chem. Rev.* 252 (2008) 2093–2114, <https://doi.org/10.1016/j.ccr.2007.11.011>.
- [34] J.-H. Cho, M. Kim, Y. You, H.-I. Lee, A new photoactivable NO-releasing (Ru–NO)₆ ruthenium nitrosyl complex with a tetradentate ligand containing aniline and pyridine moieties, *Chem. Asian J.* 17 (2022) e202101244.
- [35] L. Bučinský, G.E. Büchel, R. Ponec, P. Ruzan, M. Breza, J. Kožíšek, M. Gall, S. Biskupić, M. Fronc, K. Schiessl, O. Cuptan, D. Prodius, C. Turta, S. Shova, D. A. Zajac, V.B. Arion, On the electronic structure of *mer,trans*-[RuCl₃(1H-indazole)₂(NO)], a hypothetical metabolite of the antitumor drug candidate KP1019: an experimental and DFT study, *Eur. J. Inorg. Chem.*, 2013, pp. 2505–2519, <https://doi.org/10.1002/ejic.201201526>.
- [36] A. Khedkar, M. Roemelt, Modern multireference methods and their application in transition metal chemistry, *Phys. Chem. Chem. Phys.* 23 (2021) 17097–17112, <https://doi.org/10.1039/D1CP02640B>.
- [37] C.J. Cramer, D.G. Truhlar, Density functional theory for transition metals and transition metal chemistry, *Phys. Chem. Chem. Phys.* 11 (2009) 10757–10816, <https://doi.org/10.1039/b907148b>.
- [38] F. Neese, M. Atanasov, G. Bistoni, D. Maganas, S. Ye, Chemistry and quantum mechanics in 2019: give us insight and numbers, *J. Am. Chem. Soc.* 141 (2019) 2814–2824, <https://doi.org/10.1021/jacs.8b13313>.
- [39] N.M. Perez, G.Y. Higashijima, V.M. Ramos, A.P. de Lima Batista, S. Nikolaou, Probing solvents effects on the absorption spectrum of oxo-centered carbonyl-triruthenium clusters, *Polyhedron* 194 (2021) 114944, <https://doi.org/10.1016/j.poly.2020.114944>.
- [40] J.M. Palasz, T.M. Porter, C.P. Kubiak, Electronic structural studies of the Ru₃(III, II,II) mixed-valent state of oxo-centered triruthenium clusters, *Inorg. Chem.* 59 (2020) 10532–10539, <https://doi.org/10.1021/acs.inorgchem.0c00881>.
- [41] J.J. Santos, S.H. Toma, R.A. Ando, P. Corio, K. Araki, Unveiling anomalous surface-enhanced resonance Raman scattering on an oxo-triruthenium acetate cluster complex by a theoretical–experimental approach, *J. Chem. Phys. C* 124 (2020) 21674–21683, <https://doi.org/10.1021/acs.jpcc.0c05560>.
- [42] C. Gaggioli, S.J.S. Alberto, C.J. Cramer, L. Gagliardi, Beyond density functional theory: the multiconfigurational approach to model heterogeneous catalysis, *ACS Catal.* 9 (2019) 8481–8502, <https://doi.org/10.1021/acscatal.9b01775>.
- [43] G.L. Manni, R.K. Carlson, S. Luo, D. Ma, J. Olsen, D.G. Truhlar, L. Gagliardi, Multiconfiguration pair-density functional theory, *J. Chem. Theory Comput.* 10 (2014) 3669–3680, <https://doi.org/10.1021/ct500483t>.
- [44] L. Gagliardi, D.G. Truhlar, G.L. Manni, R.K. Carlson, C.E. Hoyer, J.L. Bao, Multiconfiguration pair-density functional theory: a new way to treat strongly correlated systems, *Acc. Chem. Res.* 50 (2016) 66–73, <https://doi.org/10.1021/acs.accounts.6b00471>.
- [45] B.G. Levine, A.S. Durden, M.P. Esch, F. Liang, Y. Shu, CAS without SCF—Why to use CASCI and where to get the orbitals, *J. Chem. Phys.* 154 (2021) 90902, <https://doi.org/10.1063/5.0042147>.
- [46] Z. Tóth, P. Pulay, Comparison of methods for active orbital selection in multiconfigurational calculations, *J. Chem. Theory Comput.* 16 (2020) 7328–7341, <https://doi.org/10.1021/acs.jctc.0c00123>.
- [47] S.R. White, R.L. Martin, Ab initio quantum chemistry using the density matrix renormalization group, *J. Chem. Phys.* 110 (1999) 4127–4130, <https://doi.org/10.1063/1.478295>.
- [48] G.K.-L. Chan, S. Sharma, The density matrix renormalization group in quantum chemistry, *Annu. Rev. Phys. Chem.* 62 (2011) 465–481, <https://doi.org/10.1146/annurev-physchem-032210-103338>.
- [49] L. Freitag, M. Reiher, The density matrix renormalization group for strong correlation in ground and excited states, *Quantum Chemistry and Dynamics of Excited States: Methods and Applications*, 2020, pp. 205–245.
- [50] K.H. Marti, M. Reiher, The density matrix renormalization group algorithm in quantum chemistry, *Z. Phys. Chem.* 224 (2010) 583–599, <https://doi.org/10.1524/zpch.2010.6125>.
- [51] J. Ivanic, Direct configuration interaction and multiconfigurational self-consistent-field method for multiple active spaces with variable occupations. I. Method, *J. Chem. Phys.* 119 (2003) 9364–9376, <https://doi.org/10.1063/1.1615954>.
- [52] D. Ma, G.L. Manni, L. Gagliardi, The generalized active space concept in multiconfigurational self-consistent field methods, *J. Chem. Phys.* 135 (2011) 44128, <https://doi.org/10.1063/1.3611401>.
- [53] G.L. Manni, D. Ma, F. Aquilante, J. Olsen, L. Gagliardi, SplitGAS method for strong correlation and the challenging case of Cr₂, *J. Chem. Theory Comput.* 9 (2013) 3375–3384, <https://doi.org/10.1021/ct400046n>.
- [54] A.E. Rask, P.M. Zimmerman, Toward full configuration interaction for transition-metal complexes, *J. Phys. Chem. A* 125 (2021) 1598–1609, <https://doi.org/10.1021/acs.jpca.0c07624>.
- [55] A.A. Holmes, N.M. Tubman, C.J. Umrigar, Heat-bath configuration interaction: an efficient selected configuration interaction algorithm inspired by heat-bath sampling, *J. Chem. Theory Comput.* 12 (2016) 3674–3680, <https://doi.org/10.1021/acs.jctc.6b00407>.
- [56] J.B. Schriber, F.A. Evangelista, Communication: an adaptive configuration interaction approach for strongly correlated electrons with tunable accuracy, *J. Chem. Phys.* 144 (2016) 161106, <https://doi.org/10.1063/1.4948308>.
- [57] N.M. Tubman, J. Lee, T.Y. Takeshita, M. Head-Gordon, K.B. Whaley, A deterministic alternative to the full configuration interaction quantum Monte Carlo method, *J. Chem. Phys.* 145 (2016) 44112, <https://doi.org/10.1063/1.4955109>.
- [58] G.H. Booth, A.J.W. Thom, A. Alavi, Fermion Monte Carlo without fixed nodes: a game of life, death, and annihilation in Slater determinant space, *J. Chem. Phys.* 131 (2009) 54106, <https://doi.org/10.1063/1.3193710>.
- [59] S. Ten-no, Stochastic determination of effective Hamiltonian for the full configuration interaction solution of quasi-degenerate electronic states, *J. Chem. Phys.* 138 (2013) 164126, <https://doi.org/10.1063/1.4802766>.
- [60] A. Baiardi, M. Reiher, The density matrix renormalization group in chemistry and molecular physics: recent developments and new challenges, *J. Chem. Phys.* 152 (2020) 40903, <https://doi.org/10.1063/1.5129672>.
- [61] B.O. Roos, P.R. Taylor, P.E.M. Sigbahn, A complete active space SCF method (CASSCF) using a density matrix formulated super-CI approach, *Chem. Phys.* 48 (1980) 157–173, [https://doi.org/10.1016/0301-0104\(80\)80045-0](https://doi.org/10.1016/0301-0104(80)80045-0).
- [62] C. Daniel, Photochemistry and photophysics of transition metal complexes: quantum chemistry, *Coord. Chem. Rev.* 282–283 (2015) 19–32, <https://doi.org/10.1016/j.ccr.2014.05.023>.
- [63] B.A. Finney, S.R. Chowdhury, C. Kirkvold, B. Vlaisavljevich, CASPT2 molecular geometries of Fe(ii) spin-crossover complexes, *Phys. Chem. Chem. Phys.* 24 (2022) 1390–1398, <https://doi.org/10.1039/D1CP04885F>.
- [64] S. Mai, F. Plasser, J. Dorn, M. Fumanal, C. Daniel, L. González, Quantitative wave function analysis for excited states of transition metal complexes, *Coord. Chem. Rev.* 361 (2018) 74–97, <https://doi.org/10.1016/j.ccr.2018.01.019>.
- [65] Y.A. Aoto, A.P. de Lima Batista, A. Köhn, A.G.S. de Oliveira-Filho, How to arrive at accurate benchmark values for transition metal compounds: computation or experiment? *J. Chem. Theory Comput.* 13 (2017) 5291–5316, <https://doi.org/10.1021/acs.jctc.7b00688>.
- [66] K. Pierloot, Q. Manh Phung, A. Ghosh, Electronic structure of neutral and anionic iron–nitrosyl corrole, a multiconfigurational and density matrix renormalization group investigation, *Inorg. Chem.* 59 (2020) 11493–11502, <https://doi.org/10.1021/acs.inorgchem.0c01312>.
- [67] Q.M. Phung, Y. Muchammad, T. Yanai, A. Ghosh, A DMRG/CASPT2 Investigation of metallocorroles: quantifying ligand noninnocence in archetypal 3d and 4d element derivatives, *JACS Au* 1 (2021) 2303–2314, <https://doi.org/10.1021/jacsau.1c00417>.
- [68] S.R. White, Density-matrix algorithms for quantum renormalization groups, *Phys. Rev. B* 48 (1993) 10345–10356, <https://doi.org/10.1103/PhysRevB.48.10345>.
- [69] S.R. White, Density matrix formulation for quantum renormalization groups, *Phys. Rev. Lett.* 69 (1992) 2863–2866, <https://doi.org/10.1103/PhysRevLett.69.2863>.
- [70] L. Freitag, L. Lindenbauer, M. Oettel, L. González, A Density matrix renormalization group study of the low-lying excited states of a molybdenum carbonyl-nitrosyl complex, *ChemPhysChem* 22 (2021) 2371–2377.
- [71] L. Freitag, L. González, The role of triplet states in the photodissociation of a platinum azide complex by a density matrix renormalization group method,

- J. Phys. Chem. Lett. 12 (2021) 4876–4881, <https://doi.org/10.1021/acs.jpcclett.1c00829>.
- [72] M. Roemelt, V. Krewald, D.A. Pantazis, Exchange coupling interactions from the density matrix renormalization group and *n*-electron valence perturbation theory: application to a biomimetic mixed-valence manganese complex, *J. Chem. Theory Comput.* 14 (2017) 166–179, <https://doi.org/10.1021/acs.jctc.7b01035>.
- [73] M. Roemelt, D.A. Pantazis, Multireference approaches to spin-state energetics of transition metal complexes utilizing the density matrix renormalization group, *Adv. Theory Simul.* 2 (2019) 1800201.
- [74] P. Sharma, J.J. Bao, D.G. Truhlar, L. Gagliardi, Multiconfiguration pair-density functional theory, *Annu. Rev. Phys. Chem.* 72 (2021) 541–564, <https://doi.org/10.1146/annurev-physchem-090419-043839>.
- [75] C. Zhou, L. Gagliardi, D.G. Truhlar, Multiconfiguration pair-density functional theory for iron porphyrin with cas, ras, and dmrg active spaces, *J. Chem. Phys. A* 123 (2019) 3389–3394, <https://doi.org/10.1021/acs.jpca.8b12479>.
- [76] L. Wilbraham, P. Verma, D.G. Truhlar, L. Gagliardi, I. Ciofini, Multiconfiguration pair-density functional theory predicts spin-state ordering in iron complexes with the same accuracy as complete active space second-order perturbation theory at a significantly reduced computational cost, *J. Phys. Chem. Lett.* 8 (2017) 2026–2030, <https://doi.org/10.1021/acs.jpcclett.7b00570>.
- [77] S.J. Stoneburner, D.G. Truhlar, L. Gagliardi, Transition metal spin-state energetics by mc-pdft with high local exchange, *J. Phys. Chem. A* 124 (2020) 1187–1195, <https://doi.org/10.1021/acs.jpca.9b10772>.
- [78] P. Sharma, D.G. Truhlar, L. Gagliardi, Magnetic coupling in a tris-hydroxo-bridged chromium dimer occurs through ligand mediated superexchange in conjunction with through-space coupling, *J. Am. Chem. Soc.* 142 (2020) 16644–16650, <https://doi.org/10.1021/jacs.0c06399>.
- [79] A.D. Becke, Density-functional thermochemistry. III. The role of exact exchange, *J. Chem. Phys.* 98 (1993) 5648–5652.
- [80] C. Lee, W. Yang, R.G. Parr, Development of the Colle-Salvetti correlation-energy formula into a functional of the electron density, *Phys. Rev. B* 37 (1988) 785–789, <https://doi.org/10.1103/PhysRevB.37.785>.
- [81] S.H. Vosko, L. Wilk, M. Nusair, Accurate spin-dependent electron liquid correlation energies for local spin density calculations: a critical analysis, *Can. J. Phys.* 58 (1980) 1200–1211, <https://doi.org/10.1139/p80-159>.
- [82] S. Grimme, S. Ehrlich, L. Goerigk, Effect of the damping function in dispersion corrected density functional theory, *J. Comp. Chem.* 32 (2011) 1456–1465.
- [83] S. Grimme, J. Antony, S. Ehrlich, H. Krieg, A consistent and accurate ab initio parametrization of density functional dispersion correction (DFT-D) for the 94 elements H-Pu, *J. Chem. Phys.* 132 (2010) 154104, <https://doi.org/10.1063/1.3382344>.
- [84] Y. Minenkov, Å. Singstad, G. Occhipinti, V.R. Jensen, The accuracy of DFT-optimized geometries of functional transition metal compounds: a validation study of catalysts for olefin metathesis and other reactions in the homogeneous phase, *Dalton Trans.* 41 (2012) 5526–5541, <https://doi.org/10.1039/C2DT12232D>.
- [85] D.R. Harper, H.J. Kulik, Computational scaling relationships predict experimental activity and rate-limiting behavior in homogeneous water oxidation, *Inorg. Chem.* 61 (2022) 2186–2197, <https://doi.org/10.1021/acs.inorgchem.1c03376>.
- [86] A.E. Kuznetsov, F.A. Thomet, A Computational approach toward organometallic ruthenium(II) compounds with tunable hydrolytic properties, *Chem. Phys.* 560 (2022) 111587, <https://doi.org/10.1016/j.chemphys.2022.111587>.
- [87] J. Yang, L. Wang, S. Zhan, H. Zou, H. Chen, M.S.G. Ahlquist, L. Duan, L. Sun, From Ru-bda to Ru-bds: a step forward to highly efficient molecular water oxidation electrocatalysts under acidic and neutral conditions, *Nat. Commun.* 12 (2021) 373, <https://doi.org/10.1038/s41467-020-20637-8>.
- [88] F. Weigend, R. Ahlrichs, Balanced basis sets of split valence, triple zeta valence and quadruple zeta valence quality for H to Rn: design and assessment of accuracy, *Phys. Chem. Chem. Phys.* 7 (2005) 3297, <https://doi.org/10.1039/b508541a>.
- [89] F. Weigend, Accurate Coulomb-fitting basis sets for H to Rn, *Phys. Chem. Chem. Phys.* 8 (2006) 1057, <https://doi.org/10.1039/b515623h>.
- [90] D.A. Pantazis, F. Neese, All-electron scalar relativistic basis sets for the 6p elements, *Theor. Chem. Acc.* 131 (2012) 1292, <https://doi.org/10.1007/s00214-012-1292-x>.
- [91] D.A. Pantazis, X.-Y. Chen, C.R. Landis, F. Neese, All-electron scalar relativistic basis sets for third-row transition metal atoms, *J. Chem. Theory Comput.* 4 (2008) 908–919, <https://doi.org/10.1021/ct800047t>.
- [92] D.A. Pantazis, F. Neese, All-electron scalar relativistic basis sets for the actinides, *J. Chem. Theory Comput.* 7 (2011) 677–684, <https://doi.org/10.1021/ct100736b>.
- [93] D.A. Pantazis, F. Neese, All-electron scalar relativistic basis sets for the lanthanides, *J. Chem. Theory Comput.* 5 (2009) 2229–2238, <https://doi.org/10.1021/ct900090f>.
- [94] F. Neese, F. Wennmohs, A. Hansen, U. Becker, Efficient, approximate and parallel Hartree–Fock and hybrid DFT calculations. A ‘chain-of-spheres’ algorithm for the Hartree–Fock exchange, *Chem. Phys.* 356 (2009) 98–109, <https://doi.org/10.1016/j.chemphys.2008.10.036>.
- [95] F. Neese, Software update: the ORCA program system, version 4.0, *WIREs Comput. Mol. Sci.* 8 (2018) e1327, <https://doi.org/10.1002/wcms.1327>.
- [96] F. Neese, The ORCA program system, *Wiley Interdiscip. Rev. Comput. Mol. Sci.* 2 (2012) 73–78, <https://doi.org/10.1002/wcms.81>.
- [97] B.O. Roos, R. Lindh, P.-Å. Malmqvist, V. Veryazov, P.-O. Widmark, New relativistic ano basis sets for transition metal atoms, *J. Phys. Chem. A* 109 (2005) 6575–6579, <https://doi.org/10.1021/jp0581126>.
- [98] N.H.F. Beebe, J. Linderberg, Simplifications in the generation and transformation of two-electron integrals in molecular calculations, *Int. J. Quantum Chem.* 12 (1977) 683–705.
- [99] R.K. Carlson, D.G. Truhlar, L. Gagliardi, Multiconfiguration pair-density functional theory: a fully translated gradient approximation and its performance for transition metal dimers and the spectroscopy of $\text{Re}_2\text{Cl}_8^{2-}$, *J. Chem. Theory Comput.* 11 (2015) 4077–4085, <https://doi.org/10.1021/acs.jctc.5b00609>.
- [100] R.K. Carlson, G.L. Manni, A.L. Sonnenberger, D.G. Truhlar, L. Gagliardi, Multiconfiguration pair-density functional theory: barrier heights and main group and transition metal energetics, *J. Chem. Theory Comput.* 11 (2015) 82–90, <https://doi.org/10.1021/ct5008235>.
- [101] F. Aquilante, J. Autschbach, A. Baiardi, S. Battaglia, V.A. Borin, L.F. Chibotaru, I. Conti, L. De Vico, M. Delcey, I. Fdez. Galván, I. Ferré, L. Freitag, M. Garavelli, X. Gong, S. Knecht, E.D. Larsson, R. Lindh, M. Lundberg, P.Å. Malmqvist, A. Nenov, J. Norell, M. Odellius, M. Olivucci, T.B. Pedersen, L. Pedraza-González, Q.M. Phung, K. Pierloot, M. Reiher, I. Schapiro, J. Segarra-Martí, F. Segatta, L. Seijo, S. Sen, D.-C. Sergentu, C.J. Stein, L. Ungur, M. Vacher, A. Valentini, V. Veryazov, Modern quantum chemistry with [Open]Molcas, *J. Chem. Phys.* 152 (2020) 214117, <https://doi.org/10.1063/5.0004835>.
- [102] I. Fdez. Galván, M. Vacher, A. Alavi, C. Angeli, F. Aquilante, J. Autschbach, J. J. Bao, S.I. Bokarev, N.A. Bogdanov, R.K. Carlson, L.F. Chibotaru, J. Creutzberg, N. Dattani, M.G. Delcey, S.S. Dong, A. Dreuw, L. Freitag, L. Manuel Frutos, L. Gagliardi, F. Gendron, A. Giussani, L. González, G. Grell, M. Guo, C.E. Hoyer, M. Johansson, S. Keller, S. Knecht, G. Kovacević, E. Källman, G. Li Manni, M. Lundberg, Y. Ma, S. Mai, J. Pedro Malhado, P. Åke Malmqvist, P. Marquetand, S.A. Mewes, J. Norell, M. Olivucci, M. Oettel, Q. Manh Phung, K. Pierloot, F. Plasser, M. Reiher, A.M. Sand, I. Schapiro, P. Sharma, C.J. Stein, L. Kragh Sørensen, D.G. Truhlar, M. Ugandi, L. Ungur, A. Valentini, S. Vancoullie, V. Veryazov, O. Weser, T.A. Wesolowski, P.-O. Widmark, S. Wouters, A. Zech, J. Patrick Zobel, R. Lindh, OpenMolcas: from source code to insight, *J. Chem. Theory Comput.* 15 (2019) 5925–5964, <https://doi.org/10.1021/acs.jctc.9b00532>.
- [103] S. Keller, M. Dolfi, M. Troyer, M. Reiher, An efficient matrix product operator representation of the quantum chemical Hamiltonian, *J. Chem. Phys.* 143 (2015) 244118.
- [104] S. Knecht, E.D. Hedegård, S. Keller, A. Kovyrshin, Y. Ma, A. Muolo, C.J. Stein, M. Reiher, New approaches for ab initio calculations of molecules with strong electron correlation, *Chimia (Aarau)* 70 (2016) 244–251.
- [105] S. Keller, M. Reiher, Spin-adapted matrix product states and operators, *J. Chem. Phys.* 144 (2016) 134101.
- [106] C.J. Stein, M. Reiher, AutoCAS: a program for fully automated multiconfigurational calculations, *J. Comput. Chem.* 40 (2019) 2216–2226.
- [107] G.M. Sheldrick, SHELXT-Integrated space-group and crystal-structure determination, *Acta Cryst.* 71 (2015) 3–8, <https://doi.org/10.1107/S2053273314026370>.
- [108] G.M. Sheldrick, A short history of SHELX, *Acta Cryst.* 64 (2008) 112–122, <https://doi.org/10.1107/S0108767307043930>.
- [109] O.V. Dolomanov, L.J. Bourhis, R.J. Gildea, J.A.K. Howard, H. Puschmann, OLEX2: a complete structure solution, refinement and analysis program, *J. Appl. Cryst.* 42 (2009) 339–341, <https://doi.org/10.1107/S0021889808042726>.
- [110] H.Y. Ye, F.R. Dai, L.Y. Zhang, Z.N. Chen, Low-valence triruthenium compounds via substitution of a bridging acetate in the parent $\text{Ru}_3\text{O}(\text{OAc})_6$ cluster core by 2,2'-azobispyridine (abpy) or 2,2'-azobis(5-chloropyrimidine) (abcp), *Inorg. Chem.* 46 (2007) 6129–6135, <https://doi.org/10.1021/ic0702771>.
- [111] D.B.G. Mateus, A.P. de Lima Batista, R.L. Rodrigues, S. Nikolaou, NO photorelease from a ruthenium complex assisted by formation of a supramolecular dimer, *J. Braz. Chem. Soc.* 31 (2020) 2319–2330, <https://doi.org/10.21577/0103-5053.20200090>.
- [112] R. da S. Vidal, F.G. Doro, K.Q. Ferreira, Z.N. da Rocha, E.E. Castellano, S. Nikolaou, E. Tfouni, Cis-trans isomerization in the syntheses of ruthenium cyclam complexes with nitric oxide, *Inorg. Chem. Commun.* 15 (2012) 93–96, <https://doi.org/10.1016/J.INOCHE.2011.09.046>.
- [113] G.F. Caramori, A.G. Kunitz, K.F. Andriani, F.G. Doro, G. Frenking, E. Tfouni, The nature of Ru-NO bonds in ruthenium tetraazamacrocyclic nitrosyl complexes - a computational study, *Dalton Trans.* 41 (2012) 7327–7339, <https://doi.org/10.1039/c2dt12094a>.
- [114] M.B. Moreira, C.F.N. Da Silva, R.B.P. Pesci, V.M. Deflon, S. Nikolaou, Revisiting oxo-centered carbonyl-triruthenium clusters: investigating CO photorelease and some spectroscopic and electrochemical correlations, *Dalton Trans.* 45 (2016) 16799–16809, <https://doi.org/10.1039/C6DT02511K>.
- [115] I. Alkorta, I. Rozas, J. Elguero, Non-conventional hydrogen bonds, *Chem. Soc. Rev.* 27 (1998) 163–170, <https://doi.org/10.1039/A827163Z>.
- [116] J. Arras, O. Ugarte Trejo, N. Bhuvanesh, C.D. McMillen, M. Stollenz, Hydrogen bonds and dispersion forces serving as molecular locks for tailored Group 11 bis (amidine) complexes, *Inorg. Chem. Front.* 9 (2022) 3267–3281, <https://doi.org/10.1039/D2QI00443G>.
- [117] B. Berti, M. Bortoluzzi, C. Cesari, C. Femoni, M.C. Iapalucci, R. Mazzoni, S. Zaccini, A comparative experimental and computational study of heterometallic Fe-M (M = Cu, Ag, Au) carbonyl clusters containing N-heterocyclic carbene ligands, *Eur. J. Inorg. Chem.* 2020 (2020) 2191–2202, <https://doi.org/10.1002/ejic.202000260>.
- [118] S. Abbas, K. Ayub, M. Sohail, S. Ali, R. Ludwig, M.A. Nadeem, S. Muhammad, Synthesis, X-ray crystal structure and spin polarized DFT study of high spin Mn based metal-organic framework, *J. Mol. Struct.* 1175 (2019) 439–444, <https://doi.org/10.1016/j.molstruc.2018.07.106>.

- [119] K. Pierloot, H. Zhao, S. Vancoillie, Copper corroles: the question of noninnocence, *Inorg. Chem.* 49 (2010) 10316–10329, <https://doi.org/10.1021/ic100866z>.
- [120] Y. Takano, T. Taniguchi, H. Isobe, T. Kubo, Y. Morita, K. Yamamoto, K. Nakasuji, T. Takui, K. Yamaguchi, Hybrid density functional theory studies on the magnetic interactions and the weak covalent bonding for the phenalenyl radical dimeric pair, *J. Am. Chem. Soc.* 124 (2002) 11122–11130, <https://doi.org/10.1021/ja0177197>.
- [121] T. Saito, Y. Kataoka, Y. Nakanishi, T. Matsui, Y. Kitagawa, T. Kawakami, M. Okumura, K. Yamaguchi, Theoretical studies on chemical bonding between Cu (II) and oxygen molecule in type 3 copper proteins, *Int. J. Quantum Chem.* 109 (2009) 3649–3658, <https://doi.org/10.1002/qua.22429>.
- [122] B.O. Roos, A.C. Borin, L. Gagliardi, Reaching the maximum multiplicity of the covalent chemical bond, *Angew. Chem. Int. Ed.* 46 (2007) 1469–1472, <https://doi.org/10.1002/anie.200603600>.
- [123] M. Radoń, E. Broclawik, K. Pierloot, Electronic structure of selected {FeNO}⁷ complexes in heme and non-heme architectures: a density functional and multireference ab initio study, *J. Chem. Phys. B* 114 (2010) 1518–1528, <https://doi.org/10.1021/jp910220r>.
- [124] F. Aquilante, L. Boman, J. Boström, H. Koch, R. Lindh, Alfredo Sánchez de Merás, Thomas Bondo Pedersen, cholesky decomposition techniques in electronic structure theory, M.G. and M.P.G. and L.J. Zalesny Robert and Papadopoulos. *Linear-Scaling Techniques in Computational Chemistry and Physics: Methods and Applications*, Springer Netherlands, Dordrecht, 2011, pp. 301–343, https://doi.org/10.1007/978-90-481-2853-2_13.
- [125] B. Possato, V.M. DeFlon, Z. Naal, A.L.B. Formiga, S. Nikolaou, An extended π -system and enhanced electronic delocalization on symmetric [Ru₃O(CH₃COO)₆(L)₃]ⁿ complexes combined with azanaphthalene ligands, *Dalton Trans.* 46 (2017) 7926–7938, <https://doi.org/10.1039/C7DT01152K>.
- [126] D.B.G. Mateus, S. da S Souza, R.J. de B Silva, A.P. de L Batista, R.S. Cicolani, V. E. Murie, R.H. Nishimura, G.C. Clososki, A.G.S. de Oliveira Filho, G.J.-F. Demets, S. Nikolaou, Assessment of the electronic structure of a triruthenium acetate-pyridyl-naphthalimide cluster, *J. Photochem. Photobiol. A* 391 (2020) 112361, <https://doi.org/10.1016/j.jphotochem.2020.112361>.
- [127] J.J. Santos, S.H. Toma, N.M. Monezi, R.A. Ando, P. Corio, K. Araki, Selecting the mechanism of surface-enhanced raman scattering effect using shell isolated nanoparticles and an oxo-triruthenium acetate cluster complex, *Inorg. Chem.* 58 (2019) 10399–10407, <https://doi.org/10.1021/acs.inorgchem.9b01618>.
- [128] T.M. Porter, G.C. Canzi, S.A. Chabolla, C.P. Kubiak, Tuning electron delocalization and transfer rates in mixed-valent Ru₃O complexes through “push-pull” effects, *J. Chem. Phys. A* 120 (2016) 6309–6316, <https://doi.org/10.1021/acs.jpca.6b05485>.
- [129] T. Porter, M.G.P. Heim, C.P. Kubiak, Stable mixed-valent complexes formed by electron delocalization across hydrogen bonds of pyrimidinone-linked metal clusters, *J. Am. Chem. Soc.* 140 (2018) 12756–12759, <https://doi.org/10.1021/jacs.8b09273>.
- [130] J.C. Goeltz, C.J. Hanson, C.P. Kubiak, Rates of electron self-exchange reactions between oxo-centered ruthenium clusters are determined by orbital overlap, *Inorg. Chem.* 48 (2009) 4763–4767, <https://doi.org/10.1021/ic8022024>.
- [131] B. Possato, Z.A. Carneiro, S. de Albuquerque, S. Nikolaou, New uses for old complexes: the very first report on the trypanocidal activity of symmetric trinuclear ruthenium complexes, *J. Inorg. Biochem.* 176 (2017) 156–158, <https://doi.org/10.1016/J.JINORGBIO.2017.08.021>.
- [132] C.F.N. da Silva, P.B.H. Chrispim, B. Possato, G.B. Portapilla, T.N. Rohrabough, L. C.B. Ramos, R. da Silva, S. de Albuquerque, C. Turro, S. Nikolaou, Anticancer and antitrypanosomal activities of trinuclear ruthenium compounds with orthometalated phenazine ligands, *Dalton Trans.* (2020), <https://doi.org/10.1039/D0DT01035A>.
- [133] B. Possato, P.B.H. Chrispim, J.Q. Alves, L.C.B. Ramos, E. Marques, A.C. de Oliveira, R.S. da Silva, A.L.B. Formiga, S. Nikolaou, Anticancer activity and DNA interaction of ruthenium acetate clusters bearing azanaphthalene ancillary ligands, *Polyhedron* 176 (2020) 114261, <https://doi.org/10.1016/j.poly.2019.114261>.

Tautomeria de Valência – dos Conceitos aos Recentes Compostos de Cobalto

Valence Tautomerism – from Concepts to Recently Cobalt Compounds

Jamile R. Pavan,^a Carlos E. T. Bruzeguini,^a Marcos A. Ribeiro^{a,*}

^aUniversidade Federal do Espírito Santo, Departamento de Química, CEP 29075-910, Vitória-ES, Brasil

*E-mail: marcos.a.ribeiro@ufes.br

Recebido: 19 de Fevereiro de 2024

Aceito: 19 de Abril de 2024

Publicado online: 2 de Maio de 2024

The development of molecular systems that switch between two states when exposed to external stimuli is a possible alternative in the construction of electronic devices that can eventually be applied in sensors, signal processors, or information storage devices. Coordination compounds that exhibit valence tautomerism have gained considerable importance due to changes in magnetic and optical properties that occur in these compounds. The changes are caused by metal-ligand electron transfer which is accompanied by a change in the spin state of the metal ion, creating two electronic states. Cobalt and *o*-dioxolene coordination compounds, with nitrogenous auxiliary ligands, represent a large part of the compounds presenting valence tautomerism. This article's main purpose is to present the characteristics of compounds that exhibit this property and to report the most recent advances in studies of mono- and dinuclear coordination compounds of this class.

Keywords: Valence tautomerism; cobalt; external stimuli; magnetic properties; *o*-dioxolenes.

1. Introdução

Obter sistemas moleculares em escala nanométrica e que sejam opticamente comutáveis é um dos principais desafios modernos da química de materiais, uma vez que esses compostos têm aplicações potenciais no desenvolvimento de novos dispositivos eletrônicos.¹⁻³ Uma atenção especial tem sido dada aos sistemas que exibem biestabilidade eletrônica, aptidão do composto em exibir dois estados eletrônicos diferentes dependendo dos parâmetros externos.⁴ Deste modo, o composto apresenta dois estados *quasi*-degenerados, próximos em energia e permutáveis reversivelmente, que resultam principalmente em propriedades ópticas e/ou magnéticas distintas entre esses estados.^{2,5,6}

Os materiais que apresentam a possibilidade de alternar entre dois estados distintos^{7,8} por meio de estímulos externos,⁶ como variação de temperatura, pressão, campo elétrico/magnético e fotoirradiação^{9,10} são investigados para serem aplicados na construção de dispositivos miniaturizados de alto desempenho,¹¹ destinados ao armazenamento de informações, processamento de sinais e sensores.¹²⁻¹⁵

Dentre os sistemas moleculares biestáveis pode-se destacar os que exibem a tautomeria de valência (TV),¹⁶⁻¹⁸ fenômeno que ocorre pela redistribuição eletrônica entre entidades redox-ativas conectadas através de ligações químicas.¹⁹

2. Tautomeria de Valência

O conceito de TV foi importante para definir as propriedades de um aduto molecular (A–D)⁺, sendo A um aceptor de elétrons e D um doador, no qual o estado eletrônico fundamental é descrito por dois ou mais isômeros com diferentes distribuições de carga.²⁰ A interconversão entre os isômeros se dá pela transferência de elétrons e pode ser representada genericamente por $A-(D^+) \rightleftharpoons (A^+)-D$.²¹

A TV em compostos de coordenação corresponde a uma transferência eletrônica intramolecular reversível entre um centro metálico e um ligante que pode exibir mais de um estado de oxidação, o ligante redox-ativo.^{22,23} Essa transferência é acompanhada por uma mudança no estado de *spin* das espécies envolvidas, criando dois estados eletrônicos distinguíveis chamados de isômeros redox ou tautômeros.^{6,24} A formação de estados eletrônicos metaestáveis de longa duração a partir de estímulos externos faz com que a TV seja objeto de estudo na aplicação em dispositivos moleculares.^{15,22}

do inglês *highest occupied molecular orbital*) está predominantemente localizado no oxigênio de posição *orto* e os orbitais *p* estão no plano do anel e representam os pares de elétrons do oxigênio, que interagem com um metal na forma de uma ligação σ .^{32,36}

No orbital molecular desocupado de mais baixa energia (LUMO, do inglês *lowest unoccupied molecular orbital*) pode-se constatar que os orbitais *p* estão perpendiculares ao plano do anel. Este é um orbital molecular antiligante π^* formado da interação entre carbono-oxigênio e que interage na forma π com o metal. É nesse orbital que se originam importantes características redox das *o*-quinonas, visto que na forma *o*-quinona esse orbital se encontra vazio, porém ao assumir as formas semiquinonato e catecolato apresentará 1 e 2 elétrons, respectivamente.³²

Dentre os sistemas que exibem tautomeria de valência, aqueles que são constituídos por íons metálicos *3d* e ligantes do tipo dioxoleno são estudados há muitos anos,^{2,6,37-39} sendo que os derivados de cobalto-*o*-dioxoleno são os mais atrativos do ponto de vista magnético.⁴⁰

Nesses sistemas, a transferência de elétrons ocorre de um ligante *o*-dioxoleno para um íon cobalto(III) *spin* baixo (do inglês *low spin*, *ls*) (t_{2g}^6), formando um composto cobalto(II) *spin* alto (do inglês *high spin*, *hs*) ($t_{2g}^5 e_g^{*2}$) coordenado agora a uma espécie *o*-dioxoleno oxidada por um elétron e com simetria octaédrica,²⁴ como representado pela Figura 2. O esquema apresentado serve de modelo básico para entendimento e interpretação das variações de propriedades.

A ocupação dos orbitais e_g^* ($d_{x^2-y^2}$ e d_z^2) na forma cobalto(II) *spin* alto resulta em uma mudança significativa nos comprimentos de ligação Co-O (cerca de 0,18 Å), o que sugere que a interconversão seja regida por fatores entrópicos.^{40,41}

Os compostos de coordenação de cobalto com ligantes *o*-dioxolenos que exibem TV podem ser representados por dois tipos. Um deles é constituído por dois ligantes redox-ativos e, para completar a esfera de coordenação octaédrica, ligantes nitrogenados mono ou bidentados. O segundo tipo apresenta um ligante redox-ativo e um ligante nitrogenado tetradentado, sendo que o uso de contraíons é necessário para estabilização.⁴²

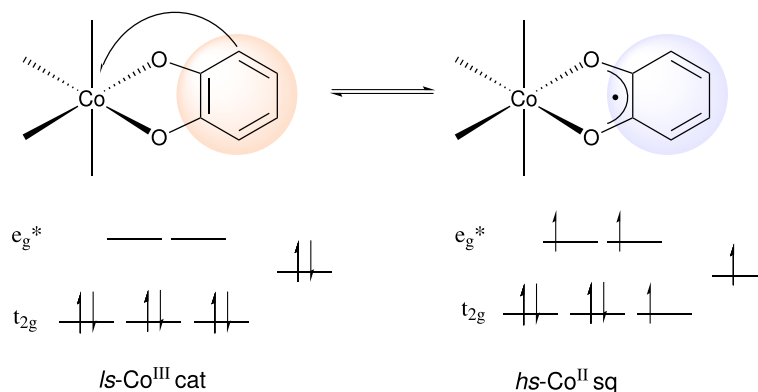


Figura 2. Transferência eletrônica intramolecular entre o íon cobalto e o ligante redox-ativo

O primeiro trabalho envolvendo TV foi relatado por Buchanan e Pierpont,³⁹ em 1980, que sintetizou um composto hexacoordenado de cobalto com o ligante redox-ativo 3,5-di-*terc*-butil-*o*-benzoquinona (dbq) e 2,2'-bipiridina (bpy) como ligante auxiliar. A dependência incomum da temperatura nas propriedades magnéticas e espectrais desse composto admitiu a existência de duas formas tautoméricas em equilíbrio,³⁸ Figura 3, e está relacionada à transferência eletrônica intramolecular. Assim, no aquecimento, um elétron é transferido do ligante diamagnético catecolato (dbcat) para o íon *ls*-Co^{III} formando um íon *hs*-Co^{II} com o ligante semiquinonato paramagnético (dbsq).²⁴

Dados termodinâmicos referentes ao equilíbrio representado na Figura 3, revelaram uma variação de entropia positiva ($\Delta S = 98 \text{ J mol}^{-1} \text{ K}^{-1}$).⁴³ Essa variação de entropia está associada ao aumento da multiplicidade de *spin* ao passar de [Co^{III}(bpy)(dbsq)(dbcat)] para [Co^{II}(bpy)(dbsq)₂] e principalmente à maior densidade de níveis vibracionais de acordo com o enfraquecimento da ligação metal-ligante na forma *hs*-Co^{II}.^{21,44} Considerando os dados entálpicos a partir da diferença de energia entre os dois níveis mais baixos de energia dado por $\Delta E = \Delta H = \Delta H_{hs\text{-Co(II)}} - \Delta H_{ls\text{-Co(III)}}$, resultando em $\Delta H = +32 \text{ kJ mol}^{-1}$,⁴³ pode-se dizer que na espécie *ls*-Co^{III} encontra-se um nível energético mais baixo do que na espécie *hs*-Co^{II}, sendo assim favorecida em baixas temperaturas. Entretanto, se ΔS for grande, a espécie *hs*-Co^{II} será predominante em temperaturas mais altas.^{21,43}

Sabendo que a transferência eletrônica intramolecular tem como consequência a mudança no comprimento de ligação metal-ligante, pode-se considerar que o comprimento é equivalente ao estiramento totalmente simétrico dos modos vibracionais Co-O. A taxa de relaxamento de um estado para o outro é controlada pela energia térmica necessária para superar a barreira de energia livre entre os dois sistemas.⁴⁵

2.2. Ligantes redox-inativos

O processo de controle e modulação da interconversão associado à TV não se limita à unidade metal-ligante redox-ativo, e pode ser influenciada pela escolha dos ânions, pelo

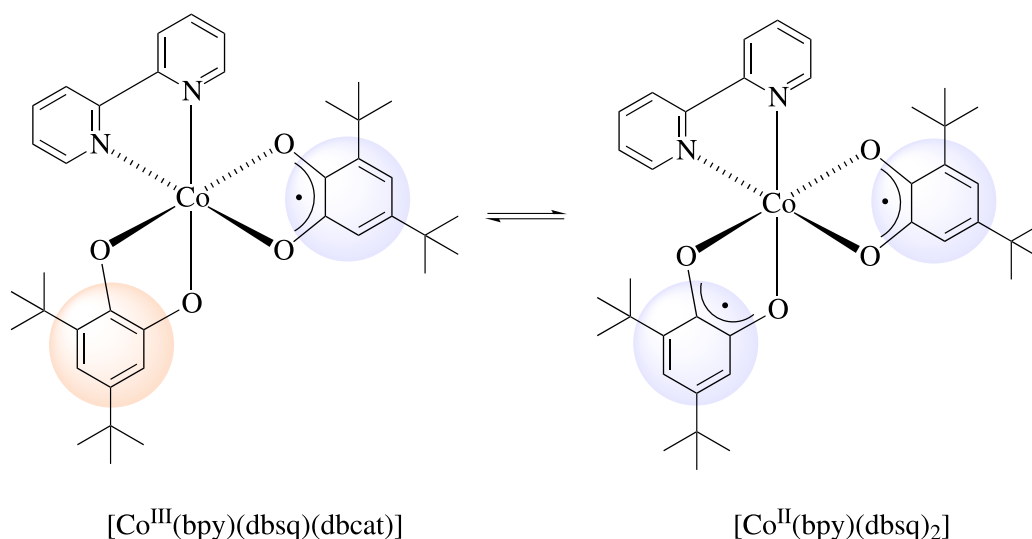


Figura 3. Equilíbrio entre as duas formas tautoméricas $[\text{Co}^{\text{III}}(\text{bpy})(\text{dbsq})(\text{dbcac})]$ e $[\text{Co}^{\text{II}}(\text{bpy})(\text{dbsq})_2]$

efeito do empacotamento cristalino,⁴⁶ presença de solvente na estrutura cristalina, interações intermoleculares^{47,48} e natureza do ligante redox-inativo. A escolha desse ligante é uma importante ferramenta usada para modular o equilíbrio tautomérico nesse sistema. Isso porque esse ligante pode alterar a separação energética entre as duas formas tautoméricas e assim, modificar a temperatura na qual as duas formas coexistem em quantidades iguais ($T_{1/2}$).⁴⁹

No intuito de investigar essa influência, Adams e Hendrickson⁴⁹ sintetizaram quatro complexos tautoméricos de valência com fórmula geral $[\text{Co}(\text{dbq})_2(\text{L})]$, em que L corresponde ao ligante nitrogenado bidentado phen (1,10-fenantrolina); bpy; dmbpy (4,4'-dimetil-2,2'-bipiridina) ou dpbpy (4,4'-difeníl-2,2'-bipiridina).

A variação do ligante nitrogenado permitiu observar que $T_{1/2}$ dependia da estrutura eletrônica desses ligantes,⁴⁹ para $[\text{Co}(\text{dbq})_2(\text{phen})]$ $T_{1/2} = 226,6$ K; $[\text{Co}(\text{dbq})_2(\text{bpy})]$ $T_{1/2} = 277,0$ K; $[\text{Co}(\text{dbq})_2(\text{dmbpy})]$ $T_{1/2} = 286,6$ K e $[\text{Co}(\text{dbq})_2(\text{dpbpy})]$ $T_{1/2} = 350,0$ K. O resultado encontrado indicou que ligantes com maiores potenciais de redução favoreciam menores $T_{1/2}$ para os compostos.^{39,49}

Essas diferentes $T_{1/2}$ estão associadas à alteração na energia do desdobramento do campo ligante Δ_o , e isso ocorre porque variações na capacidade σ doadora do ligante interferem diretamente no nível energético dos orbitais e_g , e a retrodoação π influencia no conteúdo energético dos orbitais moleculares formados com o orbital atômico t_{2g} do íon metálico.^{25,39}

A partir disso, a dependência do potencial de redução pode ser entendida pelo fato de que potenciais de redução mais positivos estão associados à menor energia dos orbitais π^* (LUMO) dos ligantes nitrogenados. Esses orbitais vazios possuem simetria adequada para interagir com orbitais metálicos ocupados do tipo π (t_{2g}). A fraca interação reduz a energia de ligação proporcionando a redução de Δ_o , assim, a retrodoação π estabiliza o tautômero na forma $hs\text{-Co}^{\text{II}}$ reduzindo $T_{1/2}$.^{32,39}

3. Tautômeros de Valência de Cobalto

A maioria dos compostos que exhibe TV relatado até hoje apresenta derivados de 3,5- e 3,6-di-*terc*-butil-*o*-benzoquinona como ligante redox-ativo. A fim de introduzir novos substituintes nas posições *orto* e *para* do anel quinona, Zolotukhin *et al.*¹⁶ sintetizaram quatro complexos mononucleares de cobalto com ligantes redox-ativos análogos. A Figura 4 representa os complexos do tipo $[\text{Co}(3,6\text{-diox})_2(\text{L})]$ obtidos, sendo **1** (3,6-diox = 3,6-isopropil-*o*-benzoquinona, L = bpy), **2** (3,6-diox = 3,6-isopropil-*o*-benzoquinona, L = phen), **3** (3,6-diox = 3,6-ciclohexil-*o*-benzoquinona, L = bpy) e **4** (3,6-diox = 3,6-ciclohexil-*o*-benzoquinona, L = phen).

Estudos das propriedades magnéticas indicaram, para os complexos **1** e **4**, momento magnético efetivo à temperatura ambiente de 2,02 e 1,87 μ_B , respectivamente. Com o resfriamento para 50 K houve uma alteração muito pequena desses valores, diminuindo aproximadamente de 0,3 μ_B . O resfriamento abaixo de 50 K resultou em uma queda acentuada do momento magnético e os valores obtidos foram próximos dos sistemas contendo um elétron desemparelhado, condizendo com complexos na forma $ls\text{-}[\text{Co}^{\text{III}}(\text{sq})(\text{cat})]$ e sem indicação de TV abaixo de 340 K.¹⁶

Para o complexo **2**, não houve alteração significativa do momento magnético entre 2–250 K, mantendo-se na forma $ls\text{-Co}^{\text{III}}(\text{sq})(\text{cat})$. O aquecimento até 340 K levou a um aumento do momento magnético, porém consideravelmente menor do que um sistema contendo íons $hs\text{-Co}^{\text{II}}$ ($S = 3/2$) e dois ligantes *o*-semiquinonatos ($S = 1/2$), o que sugere uma transformação tautomérica de valência incompleta a 340 K.

Para o complexo **3**, o valor do momento magnético revelou a forma tautomérica $ls\text{-Co}^{\text{III}}(\text{sq})(\text{cat})$ entre 2–160 K e um aumento acentuado do momento magnético entre 160–260 K indicou a interconversão tautomérica,

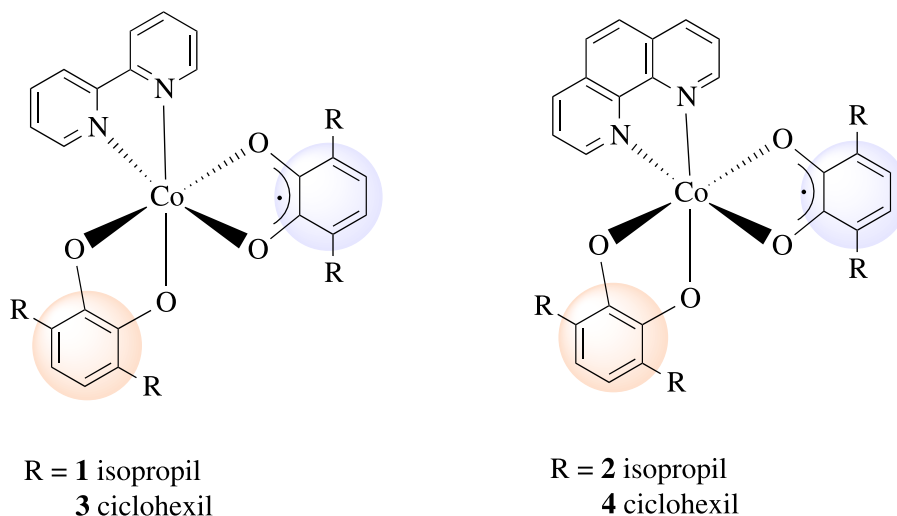


Figura 4. Complexos mononucleares de cobalto do tipo $[\text{Co}(3,6\text{-diox})_2(\text{L})]$ sintetizados por Zolotukhin *et al.*¹⁶

cujo valor à temperatura ambiente se refere à forma $[\text{hs-Co}^{\text{II}}(\text{sq})_2]$.¹⁶

A obtenção de dois novos complexos que exibem TV, **2** e **3**, com ligantes redox-ativos diferentes dos que são comumente utilizados, sugere outras possibilidades de sínteses para a investigação do fenômeno da TV.

Até aqui, foram dados como exemplos sistemas mononucleares de cobalto e que podem alternar entre dois estados eletrônicos distintos porém, apesar de menos relatado,⁴⁶ também é possível obter sistemas que realizam essa interconversão em duas etapas, em que cada centro metálico sofre a transferência de elétrons separadamente, o que os tornam interessantes em processos mais complexos.⁵⁰

Esse tipo de interconversão pode ser obtido em complexos dinucleares com ligantes tetraoxolenos (di-*o*-quinona) que, por possuírem quatro átomos de oxigênio, atuam como ligantes bis-bidentados.⁵¹ A TV em duas etapas pode ser representada pela Figura 5 que mostra um complexo dinuclear de cobalto com ligante tetraoxoleno e seus diferentes estados de oxidação em cada etapa.

A comunicação entre os dois centros metálicos por

meio da estrutura eletrônica do ligante redox-ativo em ponte permite controlar o processo de interconversão em duas etapas. Para que isso ocorra é fundamental uma escolha criteriosa do ligante em ponte, e potenciais redox do íon metálico e do ligante redox-ativo que sejam correspondentes. O estado de *spin* desses complexos também pode ser controlado pela geometria e parâmetros eletrônicos dos ligantes auxiliares.^{51,52}

Um dos ligantes redox-ativos utilizados para a investigação desse tipo de interconversão é o composto 2,5-dihidroxi-1,4-benzoquinona (DHBQ) que pode assumir vários estados de oxidação e assim formar espécies com cargas entre 4- e 1-, como sugerido na Figura 6.^{51,53}

Complexos dinucleares de cobalto com ligantes DHBQ já foram sintetizados,⁵⁴ no entanto, uma interconversão tautomérica em duas etapas não foi observada nesses sistemas, o que pode estar relacionado à interação de troca muito forte entre os dois centros magnéticos do ligante tetraoxoleno, restringindo suas capacidades redox necessárias para mais estados de valência.⁸

Para alcançar a interconversão em duas etapas, uma estratégia adotada está relacionada em inserir um ligante

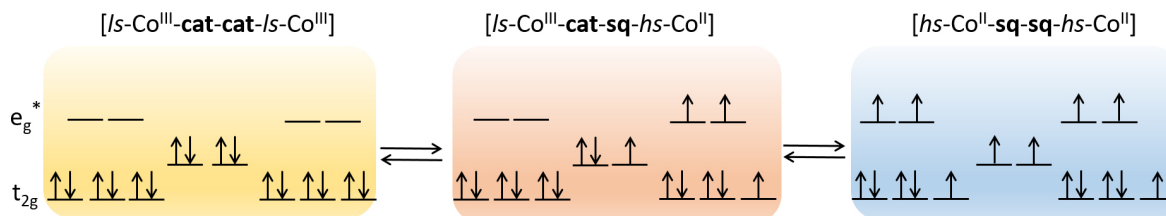


Figura 5. Representação esquemática da tautomeria de valência em duas etapas em compostos dinucleares de cobalto com ligante tetraoxoleno

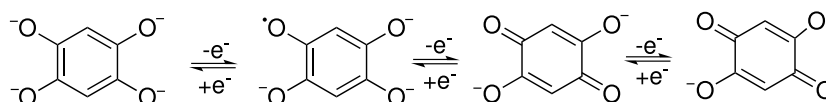


Figura 6. Reações redox possíveis no DHBQ

entre os dois centros do ligante tetraoxoleno, a fim de estabilizar o sistema **sq-sq**.⁸ Exemplos desses ligantes são os bis-bidentados de bis-dioxoleno derivados de 3,3,3',3'-tetrametil-1,1'-spiro-bis-indano-5,5',6,6'-tetrol (spiroH₄), que podem se coordenar ao metal nos estados redox **cat-cat**, **cat-sq** e **sq-sq**, ampliando assim as possibilidades de interconversão no composto de coordenação. Uma série de complexos dinucleares de cobalto com o ligante spiroH₄ e ligantes auxiliares derivados da tris(2-piridilmetil)amina (tpa), Figura 7, foi sintetizado.⁵²

A estratégia adotada pelos autores se baseou na variação do ligante redox-inativo por meio de sucessivas metilações na posição 6 dos anéis de piridina, visto que a adição de grupos metila nessa posição aumenta o impedimento estérico no centro metálico,⁵⁵ isso faz com que suas propriedades redox sejam moduladas, controlando assim a distribuição de carga da espécie cobalto-*o*-dioxoleno.

Dados da suscetibilidade magnética em diferentes temperaturas indicam complexos $[\{ls-Co^{III}(tpa)\}_2spiro^{cat-cat}]^{2+}$ e $[\{hs-Co^{II}(Me_3tpa)\}_2spiro^{sq-sq}]^{2+}$ invariantes à temperatura. Para o complexo com ligante auxiliar Me₂tpa, foi observada a variação da suscetibilidade magnética que condiz com uma sequência de duas etapas, ocorrendo em cada metade da molécula a partir da menor temperatura $[\{ls-Co^{III}(Me_2tpa)\}_2spiro^{cat-cat}]^{2+}$ para $[hs-Co^{II}(Me_2tpa)spiro^{sq-cat}ls-Co^{III}(Me_2tpa)]^{2+}$ e finalmente $[\{hs-Co^{II}(Me_2tpa)\}_2spiro^{sq-sq}]^{2+}$. Esse comportamento permitiu uma estimativa dos parâmetros termodinâmicos relevantes.⁵²

O estudo relatado indicou a possibilidade de estimular uma interconversão tautomérica de duas etapas ajustando quimicamente as interações eletrônicas. Baseando-se nesse fato e tentando elucidar os parâmetros que influenciam o

sistema a exibir transições TV de uma ou duas etapas, quatro complexos dinucleares de cobalto com os ligantes redox-ativos spiroH₄ e Br₄spiroH₄, Figura 7, e ligante auxiliar Me_ntpa (n = 0, 2 e 3) foram sintetizados.

Por meio das caracterizações dos compostos obtidos, $[\{Co(X)_2(Y)\}(PF_6)_2]$ sendo **1a** (X = Me₂tpa Y = spiro), **2a** (X = tpa Y = Br₄spiro), **3a** (X = Me₂tpa Y = Br₄spiro) e **4a** (X = Me₃tpa Y = Br₄spiro), foram observados diferentes comportamentos TV, resultando em TV parcial de uma etapa para o composto **4a** $[hs-Co^{II}(Me_3tpa)Br_4spiro^{sq-cat}ls-Co^{III}(Me_3tpa)]^{2+} \rightleftharpoons [\{hs-Co^{II}(Me_3tpa)\}_2Br_4spiro^{sq-sq}]^{2+}$, TV de duas etapas para **1a** $[\{ls-Co^{III}(Me_2tpa)\}_2spiro^{cat-cat}]^{2+} \rightleftharpoons [hs-Co^{II}(Me_2tpa)spiro^{sq-cat}ls-Co^{III}(Me_2tpa)]^{2+} \rightleftharpoons [\{hs-Co^{II}(Me_2tpa)\}_2spiro^{sq-sq}]^{2+}$, TV incompleta para **3a** $[\{ls-Co^{III}(Me_2tpa)\}_2Br_4spiro^{cat-cat}]^{2+} \rightleftharpoons [hs-Co^{II}(Me_2tpa)Br_4spiro^{sq-cat}ls-Co^{III}(Me_2tpa)]^{2+}$ e estados invariantes com o aumento da temperatura para **2a** $[\{ls-Co^{III}(tpa)\}_2Br_4spiro^{cat-cat}]^{2+}$. Esse resultado sugere que o perfil da interconversão é direcionado pelo grau de interação eletrônica dentro do ligante redox-ativo e a semelhança dos potenciais redox do íon metálico e o ligante redox-ativo.

Os casos relatados de sistemas que exibem TV com interconversão em duas etapas focam na utilização de ligantes auxiliares nitrogenados tetradentados do tipo **tpa**, porém complexos de cobalto com ligantes redox-inativos bidentados também estão sendo investigados. Complexos com ligantes bpy e 2,2'-bipiridil amina (bpa) e como ligante redox-ativo DHBQ foram sintetizados e apesar dos resultados das análises estruturais por cristalografia e propriedades magnéticas não indicarem TV em nenhum dos dois complexos, o trabalho fornece subsídios para as próximas sínteses utilizando ligantes nitrogenados bidentados terminais.⁵⁶

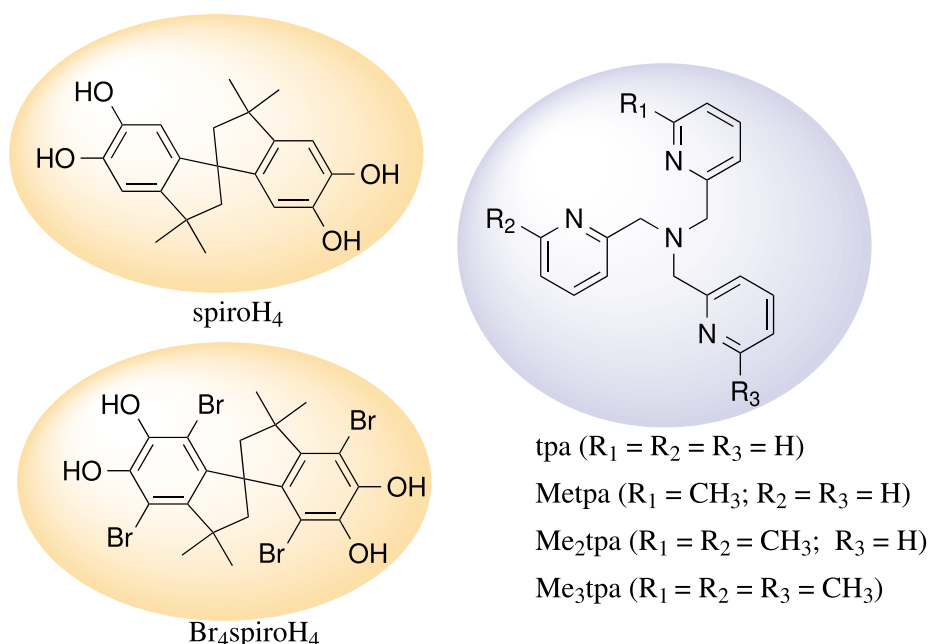


Figura 7. Ligantes redox-ativos e auxiliares utilizados na síntese de complexos dinucleares de cobalto

Para que ocorra TV de duas etapas, as energias dos orbitais d do cobalto em $\{\text{Co}^{\text{II}}(\text{L})\}$ e $\{\text{Co}^{\text{III}}(\text{L})\}$ (L = ligante redox-inativo) devem ser semelhantes às energias dos orbitais de fronteira do ligante redox-ativo em todos os três estados (**cat-cat**), (**cat-sq**) e (**sq-sq**). Tais sistemas requerem que o grau de interação eletrônica entre as unidades que apresentam tautomeria de valência seja pequeno, mas diferente de zero, de modo que cada estado possa ser acessado individualmente.⁵⁷

Até 2021, havia o relato de apenas esses dois sistemas de TV em duas etapas. Em 2022, porém, Wang *et al.*,⁸ diante da proposta que para que ocorra duas etapas seja preferencial a comunicação eletrônica intraligante fraca, resolveram estudar a possibilidade de TV em duas etapas em sistemas mais fortemente acoplados eletronicamente. Para isso, foi utilizado pela primeira vez o ligante 2,7-di-*tert*-butilpireno-4,5,9,10-tetraoxoleno. A Figura 8 mostra, de uma forma genérica, os compostos de cobalto com o novo ligante redox-ativo em ponte variando o ligante auxiliar, sendo que para o composto **1** foi utilizado phen e para **2**, bpy.

Medidas de suscetibilidade magnética em função da temperatura, e difração de raios X em monocristal indicaram que o composto **1** apresentava uma interconversão parcial de uma etapa, e no composto **2** houve uma interconversão de duas etapas, sendo este o terceiro exemplo de TV em duas etapas.⁸

O diferente comportamento ao modificar o ligante auxiliar foi atribuído à maior rigidez estérica do ligante phen em relação à bpy. Além do fator estérico, a capacidade do ligante auxiliar em aceitar elétrons também é um fator importante, e pode ser demonstrada por meio dos seus potenciais de redução. O maior potencial de redução para phen explica a sua maior capacidade de aceitação de elétrons π , e como consequência uma menor $T_{1/2}$. Destaca-se também que a interconversão de duas etapas pode ser controlada por

solvente, temperatura e luz, fundamental para potenciais aplicações em dispositivos moleculares.⁸

O trabalho em questão representa o segundo sistema que apresenta esse comportamento das propriedades magnéticas, visto que os dois outros exemplos estão relacionados ao mesmo ligante redox-ativo, o ligante do tipo spiro.

4. Casos Raros da Tautomeria de Valência: Cobalto(II) *spin* baixo

Os sistemas apresentados nessa revisão, envolvendo o íon cobalto e ligantes do tipo *o*-dioxoleno, ao transferir um elétron do ligante catecolato para o íon $ls\text{-Co}^{\text{III}}$ formam um íon $hs\text{-Co}^{\text{II}}$ com o ligante semiquinonato paramagnético.²⁴

Entretanto, em 2023, foi relatado o primeiro exemplo de TV em que um composto de coordenação de cobalto(II) assume a configuração de *spin* baixo. Nesse exemplo, o composto $[\text{Co}^{\text{II}}(\text{LN}_4^t\text{Bu}_2)(\text{Cl}_2\text{cat})]^+$; ($\text{LN}_4^t\text{Bu}_2 = \text{N}, \text{N}'$ -di-*tert*-butil-2,11-diaza[3.3](2,6)piridinofano, $\text{Cl}_2\text{cat} = 4,5$ -diclorocatecolato) transita de $ls\text{-}[\text{Co}^{\text{III}}(\text{cat})]$ para $ls\text{-}[\text{Co}^{\text{II}}(\text{sq})]$ ao aumentar a temperatura.¹⁸

Paralelamente a esse estudo, um grupo de pesquisadores apresentou um sistema em que a substituição de ligantes nitrogenados *trans*-4-estirilpiridina do composto de coordenação Co^{II} – bis-dioxoleno pelo ligante cianeto, resultou em uma rara TV entre dois íons cobalto de *spin* baixo, $ls\text{-}[\text{Co}^{\text{III}}(\text{sq})(\text{cat})]$ e $ls\text{-}[\text{Co}^{\text{II}}(\text{sq})_2]$.⁵⁸

Essa condição atípica pode ser explicada pela proximidade de energia entre os estados $ls\text{-}[\text{Co}^{\text{III}}(\text{cat})]$, $hs\text{-}[\text{Co}^{\text{II}}(\text{sq})]$ e $ls\text{-}[\text{Co}^{\text{II}}(\text{sq})]$, assim, a diferença de energia entre esses estados pode ser influenciada por diferentes fatores como: tipo de solvente, substituintes ligados ao dioxoleno, tipo de contraíons e a presença de moléculas de solventes na rede cristalina.¹⁸

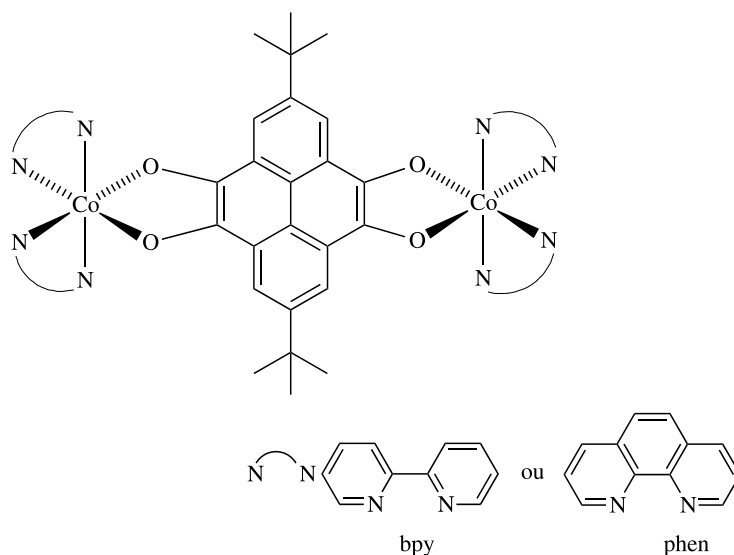


Figura 8. Compostos dinucleares de cobalto com o ligante redox-ativo 2,7-di-*tert*-butilpireno-4,5,9,10-tetraoxoleno sintetizados por Wang, J.P *et al.*⁸

5. Considerações Finais

Diante do que foi abordado até aqui, o estudo da TV busca por informações sobre os fatores que afetam a transferência eletrônica intramolecular nesses compostos, a fim de construir sistemas que, através das variações nas propriedades magnéticas e espectroscópicas ocorridas durante a interconversão tautomérica, possam contribuir para o desenvolvimento de materiais funcionais.

Baseando-se nisso, a química de complexos contendo ligantes derivados de *o*-dioxolenos e ligantes auxiliares nitrogenados tetradentados vem sendo amplamente discutida, isso porque a estrutura eletrônica desses compostos oferece excepcional labilidade, proporcionando condições para a modulação das propriedades por meio de estímulos externos. Essa característica cria perspectivas para a construção de uma variedade de complexos com propriedades magnéticas únicas.⁵¹

Agradecimentos

Ao Instituto Federal do Espírito Santo (IFES), à Coordenação de Aperfeiçoamento de Pessoal de Nível Superior (CAPES) e à Fundação de Amparo à Pesquisa do Estado do Espírito Santo (FAPES) edital 922/2023. Agradecem também a gentileza do Prof. Wdeson Pereira Barros do Instituto de Química da Unicamp na confecção do *graphical abstract*.

Referências Bibliográficas

- Kahn, O.; Martinez, C. J.; Spin-transition polymers: From molecular materials toward memory devices. *Science* **1998**, *279*, 44. [Crossref]
- Carbonera, C.; Dei, A.; Létard, J. F.; Sangregorio, C.; Sorace, L.; Thermally and light-induced valence tautomeric transition in a dinuclear cobalt-tetraoxolene complex. *Angewandte Chemie - International Edition* **2004**, *43*, 3136. [Crossref]
- Aviram, A.; Ratner, M. A.; Molecular rectifiers. *Chemical Physics Letters* **1974**, *29*, 277. [Crossref]
- Pour, Y. S.; Safaei, E.; Wojtczak, A.; Jagličić, Z.; Valence tautomerism in catecholato cobalt Bis(phenolate) diamine complexes as models for Enzyme–substrate adducts of catechol dioxygenases. *Polyhedron* **2020**, *187*, 114620. [Crossref]
- Sato, O.; Dynamic molecular crystals with switchable physical properties. *Nature Chemistry* **2016**, *8*, 644. [Crossref]
- Sato, O.; Tao, J.; Zhang, Y. Z.; Control of magnetic properties through external stimuli. *Angewandte Chemie - International Edition* **2007**, *46*, 2152. [Crossref]
- Kiriya, D.; Chang, H.-C.; Kamata, A.; Kitagawa, S.; Polytropic phase transition in alkyl chain-functionalized valence tautomeric complexes. *Dalton Transactions* **2006**, *60*, 1377. [Crossref]
- Wang, J.-P.; Liu, W.-T.; Yu, M.; Ji, X.-Y.; Liu, J.-L.; Chi, M.-Z.; Starikova, A. A.; Tao, J.; One-Step versus Two-Step Valence Tautomeric Transitions in Tetraoxolene-Bridged Dinuclear Cobalt Compounds. *Inorganic Chemistry* **2022**, *61*, 4428. [Crossref][PubMed]
- Schmidt, R. D.; Shultz, D. A.; Martin, J. D.; Magnetic Bistability in a Cobalt Bis(dioxolene) Complex: Long-Lived Photoinduced Valence Tautomerism. *Inorganic Chemistry* **2010**, *49*, 3162. [Crossref]
- Zaware, S. B.; Dagade-Waghmode, S.; Gonnade, R. G.; Srinivas, D.; Rane, S. Y.; Magnetic phase transition in valence tautomers as polymorphs of 3-iodolawsone: Single crystal X-ray structure, DSC and EPR studies. *Journal of Molecular Structure* **2009**, *938*, 328. [Crossref]
- Kiriya, D.; Chang, H.-C.; Kitagawa, S.; Molecule-Based Valence Tautomeric Bistability Synchronized with a Macroscopic Crystal-Melt Phase Transition. *Journal of the American Chemical Society* **2008**, *130*, 5515. [Crossref]
- Chang, H. C.; Kiriya, D.; Synchronic transformations of molecular states and macroscopic phases in valence-tautomeric complexes. *European Journal of Inorganic Chemistry* **2013**, *2013*, 642. [Crossref]
- Jana, N. C.; Qi, X. H.; Brandão, P.; Mathonière, C.; Panja, A.; Impact of Positional Isomers on the Selective Isolation of cis-trans Isomers in Cobalt-Dioxolene Chemistry and Solvation Effects on the Valence Tautomerism in the Solid State. *Crystal Growth and Design* **2022**, *22*, 993. [Crossref]
- Guasch, J.; Grisanti, L.; Jung, S.; Morales, D.; D'Avino, G.; Souto, M.; Fontrodona, X.; Painelli, A.; Renz, F.; Ratera, I.; Veciana, J.; Bistability of Fc-PTM-Based dyads: The role of the donor strength. *Chemistry of Materials* **2013**, *25*, 808. [Crossref]
- Calzolari, A.; Chen, Y.; Lewis, G. F.; Dougherty, D. B.; Shultz, D.; Buongiorno Nardelli, M.; Complex materials for molecular spintronics applications: Cobalt bis(dioxolene) valence tautomers, from molecules to polymers. *Journal of Physical Chemistry B* **2012**, *116*, 13141. [Crossref]
- Zolotukhin, A. A.; Bubnov, M. P.; Skorodumova, N. A.; Kocherova, T. N.; Bogomyakov, A. S.; Kozlova, E. A.; Fukin, G. K.; Cherkasov, V. K.; Valence tautomerism in cobalt complexes based on isopropyl- and cyclohexyl-substituted *o*-quinones. *Inorganica Chimica Acta* **2022**, *534*, 120811. [Crossref]
- Evangelio, E.; Ruiz-Molina, D.; Valence tautomerism: New challenges for electroactive ligands. *European Journal of Inorganic Chemistry* **2005**, *2005*, 2957. [Crossref]
- Metzger, C.; Dolai, R.; Reh, S.; Kelm, H.; Schmitz, M.; Oelkers, B.; Sawall, M.; Neymeyr, K.; Krüger, H. J.; A New Type of Valence Tautomerism in Cobalt Dioxolene Complexes – Temperature-Induced Transition from a Cobalt(III) Catecholate to a Low-Spin Cobalt(II) Semiquinonate State. *Chemistry - A European Journal* **2023**, *29*, e202300091. [Crossref] [PubMed]
- Chen, J.; Wuttke, E.; Polit, W.; Exner, T.; Winter, R. F.; Simultaneous Occurrence of Three Different Valence Tautomers in meso -Vinylruthenium-Modified Zinc Porphyrin Radical Cations. *Journal of the American Chemical Society* **2013**, *135*, 3391. [Crossref] [PubMed]
- Goswami, S.; Panja, A.; Butcher, R. J.; Shaikh, N.; Banerjee, P.; Ligand-to-ligand electron transfer and temperature induced

- valence tautomerism in o-dioxolene chelated manganese complexes. *Inorganica Chimica Acta* **2011**, *370*, 311. [[Crossref](#)]
21. Gütlich, P.; Dei, A.; Valence Tautomeric Interconversion in Transition Metal 1,2-Benzoquinone Complexes. *Angewandte Chemie (International Edition in English)* **1997**, *36*, 2734. [[Crossref](#)]
 22. Liang, H. W.; Kroll, T.; Nordlund, D.; Weng, T.-C.; Sokaras, D.; Pierpont, C. G.; Gaffney, K. J.; Charge and Spin-State Characterization of Cobalt Bis(o-dioxolene) Valence Tautomers Using Co K β X-ray Emission and L-Edge X-ray Absorption Spectroscopies. *Inorganic Chemistry* **2017**, *56*, 737. [[Crossref](#)] [[PubMed](#)]
 23. Fleming, C.; Chung, D.; Ponce, S.; Brook, D. J. R.; Daros, J.; Das, R.; Ozarowski, A.; Stoian, S. A.; Valence tautomerism in a cobalt-verdazyl coordination compound. *Chemical Communications* **2020**, *56*, 4400. [[Crossref](#)] [[PubMed](#)]
 24. Tezgerevska, T.; Alley, K. G.; Boskovic, C.; Valence tautomerism in metal complexes: Stimulated and reversible intramolecular electron transfer between metal centers and organic ligands. *Coordination Chemistry Reviews* **2014**, *268*, 23. [[Crossref](#)]
 25. Hendrickson, D. N.; Pierpont, C. G.; Valence Tautomeric Transition Metal Complexes. **2004**, *1*, 63. [[Crossref](#)]
 26. Ando, I.; Fukuishi, T.; Ujimoto, K.; Kurihara, H.; Oxidation states and redox behavior of ruthenium ammine complexes with redox-active dioxolene ligands. *Inorganica Chimica Acta* **2012**, *390*, 47. [[Crossref](#)]
 27. Greb, L.; Valence Tautomerism of p-Block Element Compounds – An Eligible Phenomenon for Main Group Catalysis? *European Journal of Inorganic Chemistry* **2022**, *2022*, e202100871. [[Crossref](#)]
 28. McNaught, A. D.; Wilkinson, A.; *IUPAC Compendium of Chemical Terminology: Gold Book*, 2a. ed., Blackwell Scientific: Oxford, 1997.
 29. Broere, D. L. J.; Plessius, R.; Van Der Vlugt, J. I.; New avenues for ligand-mediated processes-expanding metal reactivity by the use of redox-active catechol, o-aminophenol and o-phenylenediamine ligands. *Chemical Society Reviews* **2015**, *44*, 6886. [[Crossref](#)]
 30. Gentili, P. L.; Bussotti, L.; Righini, R.; Beni, A.; Bogani, L.; Dei, A.; Time-resolved spectroscopic characterization of photo-induced valence tautomerism for a cobalt-dioxolene complex. *Chemical Physics* **2005**, *314*, 9. [[Crossref](#)]
 31. Carbonera, C.; Dei, A.; Létard, J. F.; Sangregorio, C.; Sorace, L.; Relaxation dynamics of a photoinduced di-cobalt-tetraoxolene valence tautomer. *Inorganica Chimica Acta* **2007**, *360*, 3825. [[Crossref](#)]
 32. Adams, D. M.; Noodleman, L.; Hendrickson, D. N.; Density Functional Study of the Valence-Tautomeric Interconversion Low-Spin [CoIII(SQ)(Cat)(phen)] -High-Spin [CoII(SQ)2(phen)]. *Inorganic Chemistry* **1997**, *36*, 3966. [[Crossref](#)]
 33. Caneschi, A.; Dei, A.; Gatteschi, D.; Tangoulis, V.; Antiferromagnetic Coupling in a Six-Coordinate High Spin Cobalt(II)-Semiquinonato Complex. *Inorganic Chemistry* **2002**, *41*, 3508. [[Crossref](#)] [[PubMed](#)]
 34. Gransbury, G. K.; Boulon, M.-E.; Mole, R. A.; Gable, R. W.; Moubaraki, B.; Murray, K. S.; Sorace, L.; Soncini, A.; Boskovic, C.; Single-ion anisotropy and exchange coupling in cobalt(II)-radical complexes: insights from magnetic and ab initio studies. *Chemical Science* **2019**, *10*, 8855. [[Crossref](#)]
 35. Himmel, H. J.; Valence tautomerism in copper coordination chemistry. *Inorganica Chimica Acta* **2018**, *481*, 56. [[Crossref](#)]
 36. Ribeiro, M. A.; *Tese de doutorado*, Universidade Federal de Minas Gerais, 2013. [[Link](#)]
 37. Sato, O.; Cui, A.; Matsuda, R.; Tao, J.; Hayami, S.; Photo-induced Valence Tautomerism in Co Complexes. *Accounts of Chemical Research* **2007**, *40*, 361. [[Crossref](#)]
 38. Buchanan, R. M.; Pierpont, C. G.; Tautomeric Catecholate-Semiquinone Interconversion via Metal-Ligand Electron Transfer. Structural, Spectral, and Magnetic Properties of (3,5-Di-tert-butylcatecholato)-(3,5-di-tert-butylsemiquinone) (bipyridyl)cobalt(III), a Complex Containing Mixed-Valence. *Journal of the American Chemical Society* **1980**, *102*, 4951. [[Crossref](#)]
 39. Shultz, D. A.; Em *Magnetism: Molecules to Materials*; Miller, J. S.; Drillon, M., eds.; Wiley-VCH Verlag GmbH & Co. KGaA: Weinheim, 2003, cap. 8. [[Crossref](#)]
 40. Dei, A.; Feis, A.; Poneti, G.; Sorace, L.; Thermodynamics of valence tautomeric interconversion in a tetrachlorodioxolene:cobalt 1:1 adduct. *Inorganica Chimica Acta* **2008**, *361*, 3842. [[Crossref](#)]
 41. Bin-Salamon, S.; Brewer, S. H.; Depperman, E. C.; Franzen, S.; Kampf, J. W.; Kirk, M. L.; Kumar, R. K.; Lappi, S.; Peariso, K.; Preuss, K. E.; Shultz, D. A.; Testing bridge-mediated differences in dinuclear valence tautomeric behavior. *Inorganic Chemistry* **2006**, *45*, 4461. [[Crossref](#)]
 42. Guda, A. A.; Chegerev, M.; Starikov, A. G.; Vlasenko, V. G.; Zolotukhin, A. A.; Bubnov, M. P.; Cherkasov, V. K.; Shapovalov, V. V.; Rusalev, Y. V.; Tereshchenko, A. A.; Trigub, A. L.; Chernyshev, A. V.; Soldatov, A. V.; Valence tautomeric transition of bis(o-dioxolene) cobalt complex in solid state and solution. *Journal of Physics: Condensed Matter* **2021**, *33*, 215405. [[Crossref](#)] [[PubMed](#)]
 43. Pierpont, C. G.; Jung, O. S.; Thermodynamic Parameters for Cobalt-Quinone Electron Transfer and Spin Transition Steps of the CoIII(bpy)(3,5-DBSQ)(3,5-DBCat)/CoII(bpy)(3,5-DBSQ)2 Valence Tautomeric Equilibrium. *Inorganic Chemistry* **1995**, *34*, 4281. [[Crossref](#)]
 44. Adams, D. M.; Dei, A.; Rheingold, A. L.; Hendrickson, D. N.; Bistability in the [CoII(semiquinonate)2] to [CoIII(catecholate) (semiquinonate)] Valence-Tautomeric Conversion. *Journal of the American Chemical Society* **1993**, *115*, 8221. [[Crossref](#)]
 45. Beni, A.; Carbonera, C.; Dei, A.; Létard, J. F.; Righini, R.; Sangregorio, C.; Sorace, L.; Optically induced valence tautomeric interconversion in cobalt dioxolene complexes. *Journal of the Brazilian Chemical Society* **2006**, *17*, 1522. [[Crossref](#)]
 46. Sundaresan, S.; Diehl, M.; Carrella, L. M.; Rentschler, E.; Triggering of Valence Tautomeric Transitions in Dioxolene-Based Cobalt Complexes Influenced by Ligand Substituents, Coligands, and Anions. *Magnetochemistry* **2022**, *8*, 109. [[Crossref](#)]
 47. Ribeiro, M. A.; Stasiw, D. E.; Pattison, P.; Raithby, P. R.; Shultz, D. A.; Pinheiro, C. B.; Toward Controlling the Solid State Valence Tautomeric Interconversion Character by Solvation.

- Crystal Growth and Design* **2016**, *16*, 2385. [[Crossref](#)]
48. Mulyana, Y.; Poneti, G.; Moubaraki, B.; Murray, K. S.; Abrahams, B. F.; Sorace, L.; Boskovic, C.; Solvation effects on the valence tautomeric transition of a cobalt complex in the solid state. *Dalton Transactions* **2010**, *39*, 4757. [[Crossref](#)] [[PubMed](#)]
49. Adams, D. M.; Hendrickson, D. N.; Pulsed laser photolysis and thermodynamics studies of intramolecular electron transfer in valence tautomeric cobalt o-quinone complexes. *Journal of the American Chemical Society* **1996**, *118*, 11515. [[Crossref](#)]
50. Reu, O.; Ostrovsky, S.; Decurtins, S.; Liu, S.; Klokishner, S.; Electric Field Control of the Valence-Tautomeric Transformation in Cobalt Complexes. *European Journal of Inorganic Chemistry* **2017**, *2017*, 5356. [[Crossref](#)]
51. Chegerev, M. G.; Starikova, A. A.; Electronic Lability of Quinonoid-Bridged Dinuclear 3 d-Metal Complexes with Tetradentate N-Donor Bases. *European Journal of Inorganic Chemistry* **2021**, *2021*, 2684. [[Crossref](#)]
52. Alley, K. G.; Poneti, G.; Robinson, P. S. D.; Nafady, A.; Moubaraki, B.; Aitken, J. B.; Drew, S. C.; Ritchie, C.; Abrahams, B. F.; Hocking, R. K.; Murray, K. S.; Bond, A. M.; Harris, H. H.; Sorace, L.; Boskovic, C.; Redox Activity and Two-Step Valence Tautomerism in a Family of Dinuclear Cobalt Complexes with a Spiroconjugated Bis(dioxolene) Ligand. *Journal of the American Chemical Society* **2013**, *135*, 8304. [[Crossref](#)] [[PubMed](#)].
53. Dei, A.; Gatteschi, D.; Pardi, L.; Russo, U.; Tetraoxolene Radical Stabilization by the Interaction with Transition-Metal Ions. *Inorganic Chemistry* **1991**, *30*, 2589. [[Crossref](#)]
54. Tao, J.; Maruyama, H.; Sato, O.; Valence tautomeric transitions with thermal hysteresis around room temperature and photoinduced effects observed in a cobalt-tetraoxolene complex. *Journal of the American Chemical Society* **2006**, *128*, 1790. [[Crossref](#)]
55. Beni, A.; Dei, A.; Laschi, S.; Rizzitano, M.; Sorace, L.; Tuning the charge distribution and photoswitchable properties of cobalt-dioxolene complexes by using molecular techniques. *Chemistry - A European Journal* **2008**, *14*, 1804. [[Crossref](#)]
56. Jana, N. C.; Brandão, P.; Mathonière, C.; Panja, A.; Synthesis, structure and magnetic properties of dinuclear cobalt-tetraoxolene complexes with bidentate terminal ligands. *Polyhedron* **2018**, *144*, 152. [[Crossref](#)]
57. Gransbury, G. K.; Livesay, B. N.; Janetzki, J. T.; Hay, M. A.; Gable, R. W.; Shores, M. P.; Starikova, A.; Boskovic, C.; Understanding the Origin of One- or Two-Step Valence Tautomeric Transitions in Bis(dioxolene)-Bridged Dinuclear Cobalt Complexes. *Journal of the American Chemical Society* **2020**, *142*, 10692. [[Crossref](#)] [[PubMed](#)]
58. Mörtel, M.; Goodner, S. J.; Oswald, J.; Scheurer, A.; Drewello, T.; Khusniyarov, M. M.; Low-spin to low-spin valence tautomeric transition in cobalt bis-dioxolenes. *Dalton Transactions* **2024**, *53*, 4098. [[Crossref](#)] [[PubMed](#)]

RELATÓRIO INDIVIDUAL DE TRABALHO Nº 36/2024 - VNI-CCTAG (11.02.33.01.08.02.04)

(Nº do Protocolo: NÃO PROTOCOLADO)

(Assinado digitalmente em 14/08/2024 12:43)
JAMILE ROCHA PAVAN
PROFESSOR DO ENSINO BASICO TECNICO E TECNOLOGICO
VNI-CCTAG (11.02.33.01.08.02.04)
Matrícula: 2453159

(Assinado digitalmente em 14/08/2024 14:05)
RAONI SCHIMITT HUAPAYA
COORDENADOR DE CURSO
VNI-CCTAG (11.02.33.01.08.02.04)
Matrícula: 1953917

Visualize o documento original em <https://sipac.ifes.edu.br/documentos/> informando seu número: **36**, ano: **2024**,
tipo: **RELATÓRIO INDIVIDUAL DE TRABALHO**, data de emissão: **13/08/2024** e o código de verificação:
7f76b5e7d2